Received 8 January 2024; revised 29 January 2024; accepted 9 February 2024. Date of publication 14 February 2024; date of current version 8 March 2024.

Digital Object Identifier 10.1109/OJCOMS.2024.3366155

Opportunistic Throughput Optimization in Energy Harvesting Dynamic Spectrum Sharing Wireless Networks

AMIRHOSSEIN TAHERPOUR [1], ABBAS TAHERPOUR [2] (Member, IEEE), TAMER KHATTAB [3] (Senior Member, IEEE), AND MOHAMED ABDALLAH [4] (Senior Member, IEEE)

[1]Department of Electrical Engineering, Columbia University, New York, NY 10027, USA

[2]Department of Electrical Engineering, Imam Khomeini International University, Qazvin 3414916818, Iran

[3]Department of Electrical Engineering, Qatar University, Doha, Qatar

[4]College of Science and Engineering, Hamad Bin Khalifa University, Doha, Qatar

CORRESPONDING AUTHOR: A. TAHERPOUR (e-mail: taherpour@ikiu.ac.ir)

This work was supported by NPRP Standard Project (NPRP-S) Thirteen (13th) Cycle under Grant NPRP13S-0201-200219 from the Qatar National Research Fund (a member of Qatar Foundation). The findings herein reflect the work, and are solely the responsibility, of the authors. Open Access funding is provided by the Qatar National Library.

ABSTRACT We investigate opportunistic transmissions in a time-slotted wireless network, emphasizing constraints arising from finite durations allocated to various network operations and the availability of energy for these operations. Each time frame (time slot) comprises three sub-frames: sensing, reporting, and either transmission or energy harvesting based on the presence or absence of the primary user. We assume a fixed duration for the transmission sub-frame within each time frame. Utilizing a time division multiple access (TDMA) protocol, we manage local sensing data reporting within each time frame; consequently, the reporting time is contingent on the number of users. As a result, with the total time allocated for sensing and reporting being fixed, a trade-off arises between the number of collaborating users and the number of samples. Additionally, energy limitations and causality lead to two scenarios for wireless network operation: energy-deficit and energy-surplus regimes. To address this complexity, we formulate an optimization problem aimed at maximizing overall network throughput while considering constraints imposed by finite durations for various network operations and energy availability. We provide analytical evidence of the convexity of the optimization problem in both energy-deficit and energy-surplus scenarios. Furthermore, we propose two algorithms designed to achieve optimal throughput for each scenario. The accuracy of our analyses is validated through Monte Carlo simulations. Numerical results demonstrate the effectiveness of our proposed approach.

INDEX TERMS Opportunistic spectrum access, energy-limited communications, energy harvesting, cognitive radios, network optimization, Internet of Things.

I. INTRODUCTION

WIRELESS connectivity has become a cornerstone in our hyper-connected world, significantly influenced by advancements like the Internet of Things (IoT) and the emergence of fifth-generation mobile networks (5G) and other advanced wireless networks. IoT, by linking a myriad of devices and sensors to the Internet, is pivotal in transforming various sectors including healthcare, agriculture, and manufacturing. This connectivity facilitates real-time monitoring and automation, leading to enhanced efficiency and improved quality of life. For instance, healthcare has seen notable improvements with IoT devices remotely monitoring patients' vital signs, ensuring timely interventions.

The deployment of 5G is a monumental stride in our connectivity landscape, enabling a range of previously infeasible applications. Its attributes of high speed, low latency, and extensive device connectivity are crucial for the effective functionality of autonomous vehicles, smart city

infrastructures, and high bandwidth immersive entertainment experiences. Moreover, wireless connectivity extends its importance to disaster response, education, and was notably instrumental during the COVID-19 pandemic in supporting remote work, telemedicine, and e-commerce, showcasing its broader societal impact [1].

The escalating demand for wireless communication amid the finite nature of the radio frequency spectrum embodies a growing challenge, especially with the onset of spectrum congestion leading to interference, reduced network capacity, and slower data speeds. This limitation hampers the potential expansion of wireless technologies. While certain segments of the spectrum remain underutilized due to outdated regulations and legacy allocations, the emergence of spectrum sensing and cognitive radios provides a glimmer of hope. Cognitive radios, characterized by their ability to detect and opportunistically utilize available frequency bands, serve as a remedy by enhancing spectrum efficiency. Known as secondary users or spectrum-aware radios (SARs), these smart devices actively monitor the spectrum environment, adjusting their operating frequency dynamically to mitigate spectrum scarcity without disrupting existing services [2], [3], [4], [5], [6].

Traditionally, the frequency spectrum is allocated to primary users (PUs), with exclusive rights to certain frequency bands. Spectrum sensing is pivotal in opportunistic spectrum access (OSA) systems, aiding SARs in detecting the presence of PU and evaluating spectrum availability. This enables the SARs to access unused spectrum segments without interfering with PU communications to enhance the spectral efficiency (SE) [7].

The collaborative framework among SARs augments system performance by reducing delays and errors in detection of spectrum availability. In collaborative spectrum sensing (CSS), SARs transmit their local data to a fusion center (FC) or central processing server (CPS) for a collective and more accurate decision. However, challenges such as latency in decision-making and increased energy consumption for CSS and reporting exist, necessitating effective solutions [8], [9], [10], [11], [12], [13].

Energy efficiency (EE) in wireless networks, given the size and battery limitations of SARs, has garnered extensive attention in research [14], [15], [16], [17], [18], [19].

The pivotal role of energy and battery life in determining the performance and efficiency of SARs is well-established, with energy harvesting emerging as a viable solution to mitigate energy constraints. By converting ambient energy from sources such as solar, thermal, or radio frequency into usable power, energy harvesting systems bolster the self-sustainability of SARs, alleviating the need for frequent battery replacements or external power sources [20], [21], [22].

Several studies have explored the integration of energy harvesting with wireless systems. For instance, in [23], the authors categorize SARs into two groups to optimize SE and EE through CSS and energy harvesting from PU's radio frequency signals. In [24], the authors delve into optimizing spectrum sensing intervals to balance energy harvesting and spectrum access, taking into account PU traffic statistics. Furthermore, an analysis of an OSA network, where SARs harvest energy while accessing the licensed spectrum, presents a model to maximize SAR network throughput [25], [26].

Various research highlights the potential of energy harvesting techniques to prolong sensor lifespans, reduce costs, and propose energy-efficient strategies for IoT devices, ultimately showcasing the promise of energy harvesting in enhancing network performance and extending battery life." [20], [27], [28], [29], [30].

This research investigates the tradeoff between SE and EE in cognitive radios utilizing CSS [14]. Additionally, optimal CSS strategies for distributed SARs with time-independent signals, based on the Neyman-Pearson criterion, are explored, along with an analysis of the impact of decoding errors when reporting data to the CPS [17]. Furthermore, optimization problems concerning the number of SARs have been addressed. In one case, the optimal number of SARs is determined by considering detection performance and usage efficiency in an objective function [18], while in another, two separate optimization problems are formulated to find the optimum number of SARs based on throughput and energy efficiency as objective functions [19].

In this paper, we delve into the operation of SARs within a time-slotted wireless network grappling with energy scarcity. Our focus pivots on leveraging energy harvesting from PU signals to alleviate this concern. We propose an optimization framework aimed at amplifying SAR throughput, mindful of the prevailing time and energy constraints. This endeavor is underpinned by a weighted CSS operation, optimizing spectrum utilization across a collaborative SAR network, facilitated by a collaborative detector. The crux of our strategy lies in orchestrating SAR data transmission solely during PU inactivity, harnessing harvested energy from PU conserved in finite-capacity batteries.

The energy status of SARs' batteries in each time frame bifurcates into two scenarios: energy deficit and energy surplus. We employ a time-slotted communication protocol for PU, aligning SARs' sensing, reporting, and transmission activities with the PU's time frame.

Our methodology earmarks a fixed transmission duration during each time frame when the PU is inactive, apportioning the residual time between local spectrum sensing and reporting. Using a TDMA protocol, SARs transmit local spectrum sensing results to the CPS. Unlike certain studies that feature a fixed spectrum sensing duration and variable data/reporting time [31], we maintain a constant transmission duration. During this transmission, and when the spectrum is deemed vacant, the SARs are eligible to transmit their data using any suitable technique.

The interplay between the number of SARs and the spectrum sensing interval unfolds as a trade-off, attributable to the elongated reporting time with a higher SAR participation in

CSS. In light of this, we delineate two optimization problems for energy-deficit and energy-surplus modes, integrating constraints on sensing quality and the restricted number of available samples per time frame. Our mathematical discourse attests to the convex nature of these optimization problems. Through simulation, we delineate the throughput function, constraints, and the receiver operating characteristic (ROC) curve, corroborating the efficacy of our mathematical analysis.

A. MOTIVATION AND MAJOR CONTRIBUTIONS

While previous work discussed in the literature above has aimed at finding the optimal results for CSS schemes, a few (if any) have considered jointly limited time and energy resources in energy harvesting OSA networks. Given that in practical systems, time and energy resources are jointly limited, our work in this paper is doubly motivated by the lack of such consideration in the literature and the need for it from a practical perspective.

In this paper, in order to model and address an efficient and more practical OSA, CSS combined with limited energy and time resources is studied and the optimization of the probability of error in such networks is investigated.

In order to have efficient spectrum sensing within a controlled time, a synchronous slotted communication protocol with fixed time frame (slot) duration is assumed to be employed by the PU. The SARs need to perform sensing, reporting results and transmitting data within the PU's time frame. A fixed part of the total time frame is dedicated for SARs' data transmission, while the rest is divided between local spectrum sensing by individual SARs and results reporting to make the final decision at a CPS.

The reporting channels between the SARs and the CPS are exploiting TDMA technique. Therefore, the limitation on the time duration for CSS results in joint constraints on the number of cooperating SARs and the number of samples used by each user for individual test statistics collection. Unlike most of the prior works, which assume fixed sensing times and variable data/reporting times, our model protects the data transmission rate by fixing its duration while tuning the durations of the two phases within the CSS duration in order to find the minimum *throughput* as a function of the number of cooperating SARs and the detection threshold at the CPS. The major contributions in this paper can be summarized as follows:

- *Novel system model:* Both time and energy resource limitations are considered while providing better protection on SAR's data transmission rate (through fixing the SARs' transmission duration) and protecting PU's quality of service (QoS) (through limiting collisions with PU caused by SARs) and generalizing the scheme for soft decision fusion rule. The CSS in OSA networks in both energy-deficit and energy-surplus regimes are modelled in a synchronous slotted communication protocol with fixed time frame duration.
- *Limited battery size:* We consider the impact of limited size constraints on the batteries used to store the harvested energy during the transmission of PU.
- *Generalized optimization parameters:* We optimize the overall OSA network throughput through tuning (i) the number of collaborating SARs in CSS and (ii) the CPS's combined detection threshold.
- *Tractable optimization model:* We model the optimization of the probability of error in CSS as a function of the aforementioned parameters and under the previously listed constraints for the two distinct energy harvesting scenarios; (i) energy-surplus (energy unconstrained) and (ii) energy-deficit (energy constrained) and analytically prove the convexity of the two optimization problems.
- *Analytical problem solution:* We solve the two convex optimization problems and obtain expressions for the optimal values of the two tuning parameters; namely, the number of collaborating SARs and decision (detection) threshold at the CPS, under the considered two energy harvesting scenarios.
- *Results verification and insights:* We compare and simulate the two optimized time-limited CSS problems under the considered two energy harvesting scenarios to verify our analytical model as well as illustrate the impact of the different parameters over the corresponding performance.

B. PAPER ORGANIZATION

The rest of the paper is organized as follows: In Section II, the assumptions and the system model are described. Section III studies the formalization and solution of the optimization schemes of the proposed models for energy-surplus and energy-deficit regimes. In Section IV, the numerical results for both scenarios are illustrated. Conclusions are drawn in Section V.

C. NOTATIONS

Boldface lower- and upper-case letters are used respectively to denote column vectors and matrices. $\mathbf{X}^T$ stands for the transpose of matrix $\mathbf{X}$. Additionally, diag$\{\mathbf{x}\}$ constitutes a square matrix with the elements of $\mathbf{x}$ along its main diagonal and zeros elsewhere. The identity matrix of size L and a vector with all elements equal to 1 are respectively denoted as $\mathbf{I}_L$ and $\mathbf{1}$. Also, $\lfloor x \rceil$ means the nearest integer to x. Finally, we use $\mathcal{CN}(\mathbf{0}, \Sigma)$ to represent the complex Gaussian distribution with zero mean and covariance matrix Σ. Furthermore, Table 1 represents the common notations used throughout the paper.

II. BASIC ASSUMPTIONS AND SYSTEM MODEL

In this section, we present the basic assumptions and system model for time-frame and collaborative decision making.

A. TIME FRAME STRUCTURE AND SARS' DATA MODEL

We assume there are N SARs sensing the spectrum to determine the state of the PU using a time-slotted spectrum access model with a total fixed frame duration span of T_F.

TABLE 1. Notations used.

Notations	Definition
N	Number of SARs
T_F, T_s, T_r, T_t, T_D	Total frame, sensing, reporting, and CSS time, respectively.
f_s	Sampling frequency.
M	Number of samples taken by each SAR.
$\mathcal{H}_1, \mathcal{H}_0$	Signal plus noise and noise only hypothesis, respectively.
η	Detection threshold for PU's presence decision.
$P_{\rm f}, P_{\rm d}$	Probability of false alarm and detection, respectively.
σ_s^2, σ_z^2	Variance of PU signal and noise, respectively.
h_i	Channel gain between PU and SAR i^{th}.
e_s, e_r, e_t, e_c	Energy consumed for sensing, reporting, transmitting data, circuit and computations at each SAR, respectively.
p_u, p_s, p_r, p_t, p_c	PU transmission power, consumed power by each SAR for sensing, power consumed for individual test statistics reporting, power consumed for transmitting data and power consumed by circuit and computation, respectively.
$E_t^h, E_t^b, E^{\rm cons}$	Harvested energy during time frame t, available energy at the start of time frame t, and energy to be consumed or required for all OSA operations, respectively.
π_0, π_1	Probabilities of PU's signal absence and presence, respectively.
$e_{\rm saved}$	Average harvested energy by SARs.
$\bar{P}_c$	Maximum limit for collision probability.
$\mathrm{diag}(\mathbf{a})$	A diagonal matrix whose diagonal elements are vector $\mathbf{a}$.

Each time frame is divided into three sub-frames as follows. First, the sensing sub-frame with a duration of T_s, during which each SAR takes M independent samples and each SAR calculates its local statistic. Second, in the reporting sub-frame with a duration of T_r, SARs report their local statistic to the CPS using a TDMA protocol for collaborative decision-making. Third is the data transmission or energy harvesting sub-frame with a duration of T_t, where data transmission happens if the sensed spectrum is vacant. However, if the collaborative decision indicates an occupied spectrum, the SARs harvest the energy of the PU during this transmission sub-frame.

The transmission/energy harvesting time, T_t, is supposed to be fixed to meet a minimum transmission data rate whenever the PU is absent. The frame structure is shown in Fig. 1. As seen in the figure, $t_r = \frac{T_r}{N}$ is the time interval assigned to SARs to report their data to the CPS. Due to the fact that T_F and T_t are fixed during each time frame, T_s or sensing time can be expressed as:

$$T_s = (T_F - T_t) - T_r = T_D - Nt_r. \tag{1}$$

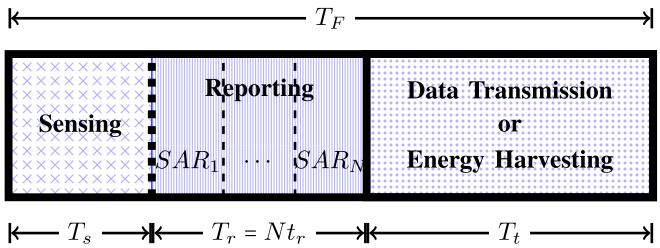

FIGURE 1. Time frame structure for the slotted system model.

where $T_D \triangleq T_s + T_r = T_F - T_t$ is the total collaborative decision time. So, for the sampling frequency of f_s, M taken samples over duration of T_s can be written as

$$M = f_s T_s = f_s(T_D - Nt_r). \tag{2}$$

It is evident that there is a trade-off between the number of SARs (N) and the number of sensing samples (M).

The received signal of each SAR at m^{th} time instance, $m = 1, \ldots, M$ under the presence or absence hypotheses, respectively denoted by $\mathcal{H}_1$ an $\mathcal{H}_0$, can be written as:

$$y_i(m) = \begin{cases} z_i(m) & , \mathcal{H}_0 \\ h_i\ s(m) + z_i(m) & , \mathcal{H}_1 \end{cases}; i = 1, 2, \ldots, N \tag{3}$$

where $y_i(m) \in \mathbb{C}^M$ is the $m^{\rm th}$ sample of the received signal sensed by $i^{\rm th}$ SAR, h_i is the channel gain between the PU and $i^{\rm th}$ SAR which is assumed to follow a flat fading distribution such that, it can be considered constant during each sensing frame. $s(m) \sim \mathcal{CN}(\mathbf{0}, \sigma_s^2\mathbf{I}_M)$ is the vector of the PU signal samples, and $z_i(m) \sim \mathcal{CN}(\mathbf{0}, \sigma_z^2\mathbf{I}_M)$ is the vector of additive noise samples at the $i^{\rm th}$ SAR.

For simplicity and convenience in detection, we assume each SAR computes the received energy as their local sensing data. Specifically, the received energy at SAR i is calculated as the sum of the squared magnitudes of the received samples, given by:

$$\theta_i \triangleq \sum_{m=1}^{M} |y_i(m)|^2 = \|\mathbf{y}_i\|^2 \tag{4}$$

Here, $y_i(m)$ represents the $m^{\rm th}$ sample received by SAR i, and $\mathbf{y}_i$ denotes the corresponding vector of received samples at SAR i^{th}.

Remark 1: It is important to note that while we assume the SARs report and utilize their local energy for CSS in the context of simplicity, the provided optimization and results are still valid and applicable even if other local decision statistics are used. As long as the local decision statistics can be inferred to follow a Gaussian distribution for a large number of samples, leveraging the central limit theorem, the optimization, and analysis can be extended accordingly.

B. COLLABORATIVE PROCESSING AND COLLECTIVE DECISION

To combat potential wireless channel impairments, a weighted (soft) combination of local decision statistics is

employed as the collaborative decision statistics to enhance the sensing operation as:

$$\Lambda_{\text{CPS}} \triangleq \sum_{i=1}^{N} w_i \theta_i = \mathbf{w}^T \theta. \tag{5}$$

where $\mathbf{w} \triangleq [w_1, w_2, \ldots, w_N]^T$ denotes combining coefficients vector and elements of $\theta \triangleq [\theta_1, \theta_2, \ldots, \theta_N]^T$ are local test statistics.

The above weighted statistic is compared with a predefined threshold η to determine the status of PU activity and hence wireless network operation mode, which could be either data transmission or energy harvesting mode:

$$\begin{cases} \mathcal{H}_0\text{: } \Lambda_{\text{CPS}} \leq \eta, \text{ Opportunistic spectrum access} \\ \mathcal{H}_1\text{: } \Lambda_{\text{CPS}} > \eta, \text{ Energy harvesting} \end{cases}, \tag{6}$$

Since the local test statistics (θ_i) are normally distributed for a large number of M, their linear combination would also be distributed normally. Consequently using (2), performance parameters of the assumed weighted detector are as follows [32],

$$P_{\text{f}} = P[\Lambda_{\text{CPS}} > \eta \mid \mathcal{H}_0] = Q\left(\frac{\eta - M\sigma_z^2 \mathbf{w}^T \mathbf{1}}{\sqrt{M\sigma_z^4 \mathbf{w}^T \mathbf{w}}}\right), \tag{7a}$$

$$P_{\text{d}} = P[\Lambda_{\text{CPS}} > \eta \mid \mathcal{H}_1] = Q\left(\frac{\eta - M\mathbf{w}^T(\sigma_s^2 \mathbf{h} + \sigma_z^2 \mathbf{1})}{\sqrt{M\sigma_z^4 \mathbf{w}^T \mathbf{C} \mathbf{w}}}\right). \tag{7b}$$

where $Q(x) \triangleq \frac{1}{\sqrt{2\pi}} \int_x^\infty \exp(-\frac{u^2}{2})\, \text{du}$ is the tail probability of standard normal distribution. $\mathbf{h} \triangleq [|h_1|^2, |h_2|^2, \ldots, |h_N|^2]^T$ and $\mathbf{C} \triangleq \text{diag}\{[\mathbf{1} + 2\boldsymbol{\gamma}]\}$ so that $\boldsymbol{\gamma} \triangleq [\gamma_1, \gamma_2, \ldots, \gamma_N]^T$, and $\gamma_i \triangleq \frac{|h_i|^2 \sigma_s^2}{\sigma_z^2}$ is the received signal-to-noise ratio (SNR) at i^{th} SAR.

C. SARS' ENERGY STORAGE AND HARVESTING MODEL

The consumed energy by the i-th SAR is expressed as:

$$E^{\text{cons,i}} = e_s^i + e_r^i + e_c^i + e_t^i P_{\text{free}}, \tag{8}$$

where

$$P_{\text{free}} = \pi_0(1 - P_{\text{f}}(N, \mathbf{w}, \eta)) + \pi_1(1 - P_{\text{d}}(N, \mathbf{w}, \eta)), \tag{9}$$

represents the probability of collaboratively deciding that the spectrum is free. Here, $e_s^i = p_s T_s$, $e_r^i = p_r t_r$, and $e_c^i = p_c T_F$ denote the energies used for sensing, reporting results of the i-th SAR, and consumed in circuit and computations, respectively. Additionally, $e_t^i = p_t T_t$ accounts for the energy required for data transmission. The probabilities π_0 and π_1 correspond to the absence and presence of the PU on the spectrum, respectively.

When a PU is active and transmitting on the channel, the SARs capture and store the harvested energy from the PU's radio frequency (RF) signal in their finite-capacity batteries. At the beginning of the subsequent time slot, this stored energy becomes available for use by the users.

To model the energy arrivals in the network, we follow the approaches proposed in [20] and [27]. Specifically, the energy arrivals are assumed to be independent and identically distributed (*i.i.d.*) random processes with a constant average arrival rate across all SARs. This average arrival rate is denoted as $\mathbb{E}[E_t^h] = e_{\text{saved}}$, which signifies the expected amount of harvested energy per time slot.

The average harvested energy can be expressed as

$$E_{t-1}^{h,i} = \zeta \pi_1 (T_D + (T_F - T_D) P_{\text{d}}) p_u |h_i|^2 \tag{10}$$

where $0 < \zeta < 1$ is the energy conversion efficiency, which is decided according to the system harvesting circuit, p_u is the transmission power of the PU, and h_i is the channel gain between PU and i^{th} SAR.

The energy stored in the battery at the beginning of each time slot ($t \in \mathbb{N}$) is governed by the equation:

$$E_t^{b,i} = \left(E_{t-1}^{b,i} + E_{t-1}^{h,i} - E_{t-1}^{\text{cons,i}}\right)^+, \quad t \geq 1, \tag{11}$$

where $(\cdot)^+ = \max\{0, \cdot\}$, $E_t^{b,i}$ represents the energy stored in the battery at the start of time frame t, and $E_{t-1}^{h,i}$ is the energy harvested by the SAR during the previous time frame, $t-1$. Each active SAR utilizes this energy for sensing and reporting in every time frame. Additionally, energy is consumed during data transmission if the spectrum is declared vacant.

Due to physical constraints, it is imperative that $E_t^{b,i} \geq 0$. Assuming a maximum battery capacity of $\mathcal{E}$, any excess harvested energy (overflow) will be wasted—i.e., not stored in the battery—when $E_t^{b,i}$ exceeds $\mathcal{E}$. Therefore, as dictated by the constraints of physics, we must also ensure $E_t^{b,i} \leq \mathcal{E}$. Assuming $P_{\text{d}} = 1$ in (10), we can deduce that the maximum energy harvested during each time slot is given by $E_h^{max} = \zeta \pi_1 T_F p_u |h_i|^2$. However, considering the finite battery capacity, it is crucial to satisfy the condition $E_h^{max} + E_0 \leq \mathcal{E}$ to ensure that, in the absence of any activity, the maximum possible harvested energy during one time frame will not be lost. Therefore, we can deduce that for the required battery capacity to enhance network energy harvesting efficiency, and consequently improve its performance, it's required

$$\mathcal{E} \geq E_0 + T_F \zeta \pi_1 p_u |h_i|^2 \tag{12}$$

Furthermore, to ensure that the battery energy remains non-negative (i.e., $E_t^{b,i} \geq 0$) at the beginning of each time frame for $t \geq 1$, each SAR performs a check to determine its operational mode. During this check, the SAR evaluates whether its stored energy is sufficient to support the three operations of sensing, reporting, and transmission (if permitted and necessary). This procedure enables the SARs to safeguard against negative energy levels, preventing potential issues. Following this check, each SAR adjusts its active state, denoted as A_t, accordingly.

$$A_t \equiv \begin{cases} 1\text{: } E_t^b \geq e_s + e_r + e_t + e_c \\ 0\text{: } E_t^b < e_s + e_r + e_t + e_c, \end{cases} \tag{13}$$

which reads: *if the energy required for all four operations in the slot* (t) *is available set* $A_t = 1$ *(become active); otherwise set* $A_t = 0$ *(remain inactive).*

The active probability is upper bounded by the normalized energy arrival rate, $\Upsilon(N, \mathbf{w}, \eta)$ [27, Appendix A].

$$\mathbb{P}(A_t = 1) \leq \min(\Upsilon(\mathrm{N}, \mathbf{w}, \eta), 1), \tag{14}$$

wherein

$$\Upsilon(N, \mathbf{w}, \eta) = \frac{e_{\text{saved}}}{E^{\text{cons}}} = \frac{e_{\text{saved}}}{e_s + e_r + e_c + e_t P_{\text{free}}} \tag{15}$$

is the ratio of the average energy arrival to the average energy consumption in active mode.

When $\Upsilon(N, \mathbf{w}, \eta) \geq 1$, indicating the SARs operate in an energy-surplus regime, it benefits from ample energy availability, resulting in throughput and PU collision constraints similar to traditional OSA networks without energy harvesting limitations.

Conversely, when $\Upsilon(N, \mathbf{w}, \eta) < 1$, the SARs function in an energy-deficit regime, where limited energy resources lead to distinct performance limitations influenced by energy causality and collision constraints.

In summary, in the energy surplus regime, performance constraints resemble those of conventional OSA networks. In contrast, the energy-deficit regime involves unique performance limitations due to energy availability and collision constraints, requiring tailored optimization approaches and parameters for each scenario to achieve optimal performance.

In the following sections, we independently tackle the optimization problem for energy-surplus and energy-deficit scenarios, presenting mathematical proofs showing that network throughput is a convex function concerning collaboration parameters (N, $\mathbf{w}$, and η) under the previously stated assumptions. Through these analyses, we provide a systematic approach to enhance wireless network performance in both energy-surplus and energy-deficit conditions, ensuring efficient spectrum resource utilization for optimal network operation.

III. OPTIMIZATION OF AVERAGE THROUGHPUT

A. ENERGY-DEFICIT MODE

In this section, we introduce an optimization problem to maximize the throughput of the wireless network while taking into account various constraints. These constraints include the limited probability of interference between the SARs' network and the PU's network, as well as a maximum number of SARs, among others. The throughput of the wireless network represents the amount of data successfully transmitted over a certain period of time. It can be quantified as the average rate of data transmission, taking into account both the data transmission duration and the probability of successful transmission.

Mathematically, we can express the throughput as the ratio of the successfully transmitted data to the total time taken for transmission. Let's denote the throughput as R, which can be formulated as follows:

$$R(N, \mathbf{w}, \eta) = \pi_0 C_t \frac{T_t}{T_F}(1 - P_{\text{f}}(N, \mathbf{w}, \eta)) \tag{16}$$

where C_t is the channel capacity. It is obvious that the probabilities of false alarm and miss detection and the throughput function should be scaled by the activity probability of the SAR. Thus,

$$\widetilde{P}_c(N, \mathbf{w}, \eta) = (1 - P_{\text{d}}(N, \mathbf{w}, \eta))\mathbb{P}(A_t = 1), \tag{17}$$

and also

$$\widetilde{R}(N, \mathbf{w}, \eta) = \pi_0 C_t \frac{T_t}{T_F}\mathbb{P}(A_t = 1)(1 - P_{\text{f}}(N, \mathbf{w}, \eta)). \tag{18}$$

In this section, our focus is on optimizing the average OSA throughput in the wireless network, taking into account a given SNR. The objective of the optimization is to maximize the average throughput while satisfying two key constraints: energy causality and interference.

The energy causality constraint ensures that the energy consumed by the SARs during each time frame does not exceed the available energy stored in their batteries. This constraint guarantees the proper operation and sustainability of the SARs within the energy constraints of the wireless network.

The interference constraint aims to limit the interference caused by the SARs' transmissions to the PU network. The SARs need to operate in a manner that minimizes the probability of interfering with the PU's communication, thereby ensuring the coexistence and efficient utilization of the spectrum by both the SARs and the PU.

By formulating the optimization problem with these constraints, we aim to find the optimal values for the parameters, such as the number of SARs, the weights for collaborative decision-making, and the threshold for determining spectrum availability. These optimized values will result in achieving the maximum average throughput while satisfying the energy causality and interference constraints.

To address the optimization problem in the energy-deficit mode while ensuring the protection of the PU against interference, we propose the following formulation:

$$\max_{N, \mathbf{w}, \eta > 0} \quad R(N, \mathbf{w}, \eta) = \pi_0 C_t \frac{T_t}{T_F}\Upsilon(N, \mathbf{w}, \eta)(1 - P_{\text{f}}(N, \mathbf{w}, \eta)) \tag{19a}$$

$$s.t.: \quad (1 - P_{\text{d}}(N, \mathbf{w}, \eta))\Upsilon(N, \mathbf{w}, \eta) \leq \bar{P}_c \tag{19b}$$

$$\Upsilon(N, \mathbf{w}, \eta) < 1 \tag{19c}$$

$$\|\mathbf{w}\|_2^2 = 1 \tag{19d}$$

$$1 \leq N \leq N_{max} \tag{19e}$$

$$\mathbf{w} \succ 0, \tag{19f}$$

where $N_{\max} = \frac{T_D}{t_r} - 1$ is obtained when the sensing time reaches its minimum value, $\bar{P}_c$ is the predefined level for interference probability that is desired to be $0 < \bar{P}_c < 0.5$, and weight coefficients ($\mathbf{w}$) are considered to have a unit norm. It is evident that the more the active state of the SAR, the more opportunities for the SAR to access the spectrum.

Consequently, the throughput is upgraded and the probability of interference is also increased. Therefore, the upper bound of the active probability is preferred to use in optimization problems in order to protect PU in the worst case.

Solving the defined optimization problem with respect to the optimization parameters $(N, \mathbf{w}, \eta)$ simultaneously can be computationally intensive. To address this, we can employ techniques to obtain the combination weights $(\mathbf{w})$ using the modified deflection coefficient. The modified deflection coefficient is a technique used to determine the weights for collaborative decision-making among the SARs. It is defined as follows:

$$d_N^2(\mathbf{w}) \triangleq \frac{(\mathbb{E}[\Lambda_{\mathrm{CPS}}|\mathcal{H}_1] - \mathbb{E}[\Lambda_{\mathrm{CPS}}|\mathcal{H}_0])^2}{Var[\Lambda_{\mathrm{CPS}}|\mathcal{H}_1]} = \frac{f_s(T_D - Nt_r)\left(\mathbf{w}^T\boldsymbol{\gamma}\right)^2}{\mathbf{w}^T\mathbf{C}\mathbf{w}} \tag{20}$$

Since the deflection coefficient is closely related to the SNR, maximizing it can lead to improved detection performance for a given probability of false alarm. Therefore, we aim to maximize the squared deflection coefficient, denoted as $d_N^2(\mathbf{w})$, while imposing a constraint on the normalized norm of the weight vector.

$$\max_{\mathbf{w}}: \ d_N^2(\mathbf{w}) \tag{21a}$$

$$s.t.: \ \|\mathbf{w}\|_2^2 = 1. \tag{21b}$$

After simplification, $d_N^2(\mathbf{w})$ can be rewritten as below from the available results originated from Rayleigh theorem [33],

$$d_N^2(\mathbf{w}) = \frac{f_s(T_D - Nt_r)\mathbf{w}'^T\mathbf{C}^{-\frac{T}{2}}\boldsymbol{\gamma}\boldsymbol{\gamma}^T\mathbf{C}^{-\frac{1}{2}}\mathbf{w}'}{\mathbf{w}'^T\mathbf{w}'} \leq f_s(T_D - Nt_r)\lambda_{max}\left(\mathbf{C}^{-\frac{T}{2}}\boldsymbol{\gamma}\boldsymbol{\gamma}^T\mathbf{C}^{-\frac{1}{2}}\right), \tag{22}$$

where $\mathbf{w}' \triangleq \mathbf{C}^{\frac{1}{2}}\mathbf{w}$. Considering the fact that equality for the above inequality will be held when $\mathbf{w}'$ equals the eigenvector corresponding to the maximum eigenvalue,

$$\mathbf{w}'_{opt} = \mathbf{C}^{-\frac{T}{2}}\boldsymbol{\gamma} \Longrightarrow \mathbf{w}_{opt} = \frac{\mathbf{C}^{-1}\boldsymbol{\gamma}}{\|\mathbf{C}^{-1}\boldsymbol{\gamma}\|}. \tag{23}$$

While this method may result in slight performance degradation, it is widely used in the statistical signal processing literature to evaluate detector performance due to its lower computational complexity.

Next, we will evaluate the convexity of the optimization problem Eq. (19) with respect to the threshold (η). It is important to note that sensing quality is of paramount importance in OSA networks. Therefore, the problem should be solved while considering the sensing performance constraints (24) and (25), which can be formulated as follows:

$$P_{\mathrm{f}} = Q(\alpha_f) < 0.5 \Longrightarrow \alpha_f > 0 \tag{24}$$

$$P_{\mathrm{d}} = Q(\alpha_d) > 0.5 \Longrightarrow \alpha_d < 0. \tag{25}$$

Streamlining the above constraints gives rise to,

$$\eta_L^s < \eta < \eta_H^s \tag{26}$$

where,

$$\eta_L^s \triangleq \frac{f_s(T_D - Nt_r)\sigma_z^2\boldsymbol{\gamma}^T\mathbf{C}^{-1}\mathbf{1}}{\|\mathbf{C}^{-1}\boldsymbol{\gamma}\|} \tag{27}$$

$$\eta_H^s \triangleq \frac{f_s(T_D - Nt_r)\boldsymbol{\gamma}^T\mathbf{C}^{-1}\left(\sigma_x^2\mathbf{h} + \sigma_z^2\mathbf{1}\right)}{\|\mathbf{C}^{-1}\boldsymbol{\gamma}\|} \tag{28}$$

Should there be a feasible set including at least one feasible point that all of the constraints be satisfied, the problem will be a convex optimization problem that can be readily solved with the available convex optimization problem solvers such as CVX in MATLAB [34]. In order to prove that the constraints form a convex set, it is necessary and sufficient to show that the constraints are convex functions with respect to η. In this regard, the convexity of constraint (19b) is discussed in Appendix C. The convexity of (19c) is proved through the following lemma.

Lemma 1: Provided that $\Phi(\eta) = \pi_0 e_t \frac{\partial^2 P_{\mathrm{f}}}{\partial \eta^2} + \pi_1 e_t \frac{\partial^2 P_{\mathrm{d}}}{\partial \eta^2} > 0$ and $max(\eta_L^{\Phi,1}, \eta_L^{\Phi,2}) < \eta < min(\eta_H^{\Phi,1}, \eta_H^{\Phi,2})$, $\Upsilon(\eta)$ is convex with respect to η. Where $\eta_L^{\Phi,1}$, $\eta_L^{\Phi,2}$, $\eta_H^{\Phi,1}$ and $\eta_H^{\Phi,2}$ are defined in (58) and (63).

Proof: See Appendix D. ■

By defining $e_f \triangleq e_s + e_r + e_c$, $x(\eta) \triangleq (1 - P_{\mathrm{f}}(\eta))$ and $y(\eta) \triangleq (1 - P_{\mathrm{d}}(\eta))$ in order to simplify analysis, concavity of cost function (19a) can be proved through the following lemma,

Lemma 2: The cost function (19a) is concave with respect to η if $\Psi_1(\eta) < 0$, $\Psi_2(\eta) < 0$, and $\eta_L^{\Psi} < \eta < \eta_H^{\Psi}$. Where, $\Psi_1(\eta)$, $\Psi_2(\eta)$, and $(\eta_L^{\Psi}, \eta_H^{\Psi})$ are defined in (67), (68), and (75), respectively.

Proof: Refer to Appendix E. ■

Therefore, the constraints and optimization problem can be reformulated on the mentioned convex sets as follows,

Problem: $\mathcal{P}'_A$

$$\max_{\eta, \mathbf{w}>0} \ \pi_0 C_t \frac{T_t}{T_F}(1 - P_{\mathrm{f}}(\eta))\Upsilon(\eta) \tag{29a}$$

$$s.t.: \ (1 - P_{\mathrm{d}}(\eta))\Upsilon(\eta) \leq \bar{P}_c \tag{29b}$$

$$\Upsilon(\eta) < 1 \tag{29c}$$

$$\Psi_1(\eta) < 0 \tag{29d}$$

$$\Psi_2(\eta) < 0 \tag{29e}$$

$$\Phi(\eta) > 0 \tag{29f}$$

$$\eta_{low} < \eta < \eta_{up} \tag{29g}$$

where η_{low} and η_{up} are,

$$\eta_{low} \triangleq \max\left(\eta_{\mathrm{L}}^{s}, \eta_{\mathrm{L}}^{\Phi,1}, \eta_{\mathrm{L}}^{\Phi,2}, \eta_{\mathrm{L}}^{\Psi}\right)$$

$$\eta_{up} \triangleq \min\left(\eta_{\mathrm{H}}^{s}, \eta_{\mathrm{H}}^{\Phi,1}, \eta_{\mathrm{H}}^{\Phi,2}, \eta_{\mathrm{H}}^{\Psi}\right). \tag{30}$$

Regarding constraint (29b), value of $\bar{P}_c$ plays an important role and both of the constraints (29b) and (29c) must be considered together. We note that $(1 - P_{\mathrm{d}}(\eta))\Upsilon(\eta)$ and $\Upsilon(\eta)$ are respectively increasing and decreasing functions of η (See Appendix B for the proof). Now if $\bar{P}_c > (1 - P_{\mathrm{d}}(\eta))$, then $(\Upsilon(\eta) < 1)$ causes limitation for threshold

and is dominant. In this case, satisfying (29c), automatically satisfies (29b), otherwise if $\bar{P}_c < (1-P_{\rm d}(\eta))$, then condition $(1-P_{\rm d}(\eta))\Upsilon(\eta) \leq \bar{P}_c$ would be dominant and it ensures us that (29c) is also satisfied. Since, $(1-P_{\rm d}(\eta))\Upsilon(\eta)$ and $\Upsilon(\eta)$ are respectively increasing and decreasing functions of η, we can simplify them to $\eta < \eta_c^{th}$ and $\eta > \eta_\Upsilon^{th}$ that η_Υ^{th} is defined as $\Upsilon(\eta_\Upsilon^{th}) = 1$ and η_c^{th} is threshold where $(1-P_{\rm d}(\eta_c^{th}))\Upsilon(\eta_c^{th}) = \bar{P}_c$.

So, two cases are considered. When, $\bar{P}_c > (1-P_{\rm d}(\eta))$, instead of (29b) and (29c) inequality $\eta > \eta_\Upsilon^{th}$ is replaced and if $\bar{P}_c$ is so that $\bar{P}_c < (1-P_{\rm d}(\eta))$, these two constraints are replaced by $\eta < \eta_c^{th}$. Now, considering constraints (29b) and (29c) together, we may address both of them in one conditional constraint as,

$$\begin{cases} \eta_{low} < \eta < \min\left(\eta_c^{th}, \eta_{up}\right); & \text{if } \ \bar{P}_c \leq (1-P_{\rm d}(\eta)) \\ \max\left(\eta_{low}, \eta_\Upsilon^{th}\right) < \eta < \eta_{up}; & \text{if } \ \bar{P}_c > (1-P_{\rm d}(\eta)) \end{cases} \tag{31}$$

In other words, should $\bar{P}_c \leq (1-P_{\rm d}(\eta))$, (29d) will be the dominant constraint and satisfies (29c), and vice-versa.

Problem: $\mathcal{P}_A^{''}$

$$\max_{\eta}: \ \pi_0 C_t \frac{T_t}{T_F}(1-P_{\rm f}(\eta))\Upsilon(\eta) \tag{32a}$$

$$s.t.: \ \Psi_1(\eta) < 0 \tag{32b}$$

$$\Psi_2(\eta) < 0 \tag{32c}$$

$$\Phi(\eta) > 0 \tag{32d}$$

$$\begin{cases} \eta_{low} < \eta < \min\left(\eta_c^{th}, \eta_{up}\right); \text{ if } \ \bar{P}_c \leq (1-P_{\rm d}(\eta)) \\ \max\left(\eta_{low}, \eta_\Upsilon^{th}\right) < \eta < \eta_{up}; \text{ if } \ \bar{P}_c > (1-P_{\rm d}(\eta)) \end{cases} \tag{32e}$$

Now, it is evident that the above optimization problem is a convex problem on η, the optimal values for the parameters η and N can be readily obtained through Algorithm 1.

Remark 2: Increasing the SNR of SARs, as per equation (7b), enhances the probability of detection ($P_{\rm d}$). In simpler terms, a higher SNR results in a monotonically increasing $P_{\rm d}$. Consequently, maintaining $\bar{P}_c$ constant, higher SNR leads to a reduced decision threshold (η). Conversely, the average energy harvesting efficiency function $\Upsilon(\eta)$ decreases with the threshold. As SNRs increase, $\Upsilon(\eta)$ reaches its maximum which is 1, removing threshold constraints and moving towards an energy-surplus regime. Additionally, for lower γ_i or SARs' SNR values, a large collaborating user count N ensures a high collective probability of correct decisions, supporting the earlier argument. In practical scenarios with numerous SARs interested in OSA and normal SNRs, $\eta_{low} < \eta_{up}$ is maintained, ensuring a non-empty feasibility set.

B. ENERGY-SURPLUS MODE

Now, provided that $(\Upsilon(N, \mathbf{w}, \eta) \geq 1)$, the upper bound of $\mathbb{P}(A_t = 1)$ will be 1. Consequently, the average throughput and the constraints are similar to the conventional OSA networks without energy harvesting ability. Therefore, by using the upper bound of inequality (14) in (18) and (17), the optimization problem over the energy-surplus mode can be formulated as follows,

Algorithm 1 Maximization of Throughput for Energy-Deficit Mode

Data: $R_0 = 0$ and $N_{max} = \frac{T_D}{t_r} - 1$
Result: R_{opt}, N_{opt}, η_{opt}
for $N = 1{:}N_{max}$ **do**
  $M \leftarrow f_s(T_D - Nt_r)$ based on (2);
  $\mathbf{w}_{opt} \leftarrow \frac{\mathbf{C}^{-1}\boldsymbol{\gamma}}{\|\mathbf{C}^{-1}\boldsymbol{\gamma}\|}$ based on (23);
  for $\eta_N = \eta_{low}{:}\eta_{up}$ **do**
    $R(\eta_N) \leftarrow \pi_0 C_t \frac{T_t}{T}(1-P_{\rm f}(\eta))\Upsilon(\eta)$;
    if $R(\eta_N) > R_0$ **then**
      $R_{opt} \leftarrow R(\eta_N)$;
      $N_{opt} \leftarrow N$;
      $\eta_{opt} \leftarrow \eta_N$;
    end
    $R_0 \leftarrow R_{opt}$
  end
end

Problem: $\mathcal{P}_B$

$$\max_{N,\mathbf{w},\eta>0}: \ \pi_0 C_t \frac{T_t}{T_F}(1-P_{\rm f}(N, \mathbf{w}, \eta)) \tag{33a}$$

$$s.t.: \ (1-P_{\rm d}(N, \mathbf{w}, \eta)) \leq \bar{P}_c \tag{33b}$$

$$\|\mathbf{w}\|_2^2 = 1 \tag{33c}$$

$$1 \leq N \leq N_{max} \tag{33d}$$

$$\mathbf{w} \succ 0, \tag{33e}$$

Indeed, minimizing the false alarm probability can lead to higher throughput. However, it is crucial to also consider the sensing quality and interference probability. Thus, the optimization problem can be reformulated as follows:

Problem: $\mathcal{P}_B'$

$$\min_{\mathbf{w},\eta>0,M}: \ P_{\rm f}(M, \mathbf{w}, \eta) \tag{34a}$$

$$s.t.: \ (1-P_{\rm d}(N, \mathbf{w}, \eta)) \leq \bar{P}_c \tag{34b}$$

$$\|\mathbf{w}\|_2^2 = 1 \tag{34c}$$

$$t_r f_s \leq M \leq f_s(T_D - Nt_r) \tag{34d}$$

$$\mathbf{w} \succ 0 \tag{34e}$$

Equation (34b) is the constraint over the threshold parameter (η) which could be simplified to $\eta \leq \eta_{opt}$. Where,

$$\eta_{opt} \triangleq Q^{-1}\left(1-\bar{P}_{\rm c}\right)\sqrt{M\sigma_v^4 \mathbf{w}^T\mathbf{C}\mathbf{w}} + M\mathbf{w}^T\left(\sigma_x^2\mathbf{h} + \sigma_z^2\mathbf{1}\right). \tag{35}$$

Also, in (34e), $\mathbf{w} \succ 0$ means all of the elements of $\mathbf{w}$ are greater than zero.

Since $P_{\rm f}(\eta)$ is a decreasing function of η, η_{opt} is the maximum value of η which satisfies the constraints and minimizes the objective function of the optimization problem (34). So, the optimization problem can be streamlined as

$$\min_{\mathbf{w},M}: \ Q\left(\frac{Q^{-1}\left(1-\bar{P}_{\rm c}\right)\sqrt{M\sigma_v^4\mathbf{w}^T\mathbf{C}\mathbf{w}} + M\sigma_x^2\mathbf{w}^T\mathbf{h}}{\sqrt{M\sigma_v^4\mathbf{w}^T\mathbf{w}}}\right) \tag{36a}$$

$$s.t.: \ f_s t_r \leq M \leq f_s(T_D - Nt_r) \tag{36b}$$

$$\|\mathbf{w}\|_2^2 = 1 \tag{36c}$$
$$\mathbf{w} \succ 0 \tag{36d}$$

Since solving the proposed optimization problem is computationally complex, we suggest employing a sub-optimal method to find an approximate global minimum. Instead of directly minimizing the objective function, we can minimize an upper bound of the objective function. Utilizing the Rayleigh-Ritz theorem and considering (36c), we can make use of the fact that $Q^{-1}(1-\bar{P}_c) < 0$, as $\bar{P}_c < \frac{1}{2}$. Therefore, we obtain:

$$Q\left(\frac{Q^{-1}\left(1-\bar{P}_c\right)\sqrt{M\sigma_v^4\mathbf{w}^T\mathbf{C}\mathbf{w}} + M\sigma_x^2\mathbf{w}^T\mathbf{h}}{\sqrt{M\sigma_v^4\mathbf{w}^T\mathbf{w}}}\right) \leq Q\left(Q^{-1}\left(1-\bar{P}_c\right)\sqrt{\lambda_{\max}(\mathbf{C})} + M'\mathbf{w}^T\boldsymbol{\gamma}\right) \tag{37}$$

where $M' \triangleq \sqrt{M}$ and $\lambda_{\max}(\mathbf{C})$ denotes the maximum eigenvalue of $\mathbf{C}$. Assuming SNRs are sorted in descending order so that $\gamma_1 \geq \gamma_2 \geq \cdots \geq \gamma_N$, $\lambda_{\max}(\mathbf{C})$ is equal to $1 + 2\gamma_1$. Minimizing the upper bound of the objective function, an accurate approximation of the optimal solution for the original problem is achieved. Thus, the new optimization problem is rewritten as follows,

Problem: $\mathcal{P}_B^{''}$

$$\min_{\mathbf{w},M'}: \; f(M',\mathbf{w}) \triangleq Q\left(Q^{-1}\left(1-\bar{P}_c\right)\sqrt{1+2\gamma_1} + M'\mathbf{w}^T\boldsymbol{\gamma}\right) \tag{38a}$$
$$s.t.: \; \sqrt{t_r f_s} \leq M' \leq \sqrt{f_s(T_D - Nt_r)} \tag{38b}$$
$$\|\mathbf{w}\|_2^2 = 1 \tag{38c}$$
$$\mathbf{w} \succ 0 \tag{38d}$$

Relaxing M' to be a continuous parameter, the convexity of this optimization problem with respect to $\mathbf{w}$ and M' can be proved through the following lemma:

Lemma 3: The optimization problem (38) is convex with respect to M' and coefficient vector $\mathbf{w}$ if $P_f(M,\mathbf{w}) \leq Q\left(\frac{1}{-Q^{-1}(1-\bar{P_C})\sqrt{1+2\gamma_1}+\sqrt{(Q^{-1}(1-\bar{P_C}))^2(1+2\gamma_1)+2}}\right)$.

Proof: See Appendix F. ■

In order to find the optimal values of $\mathbf{w}$ and N the desired convex optimization problem (38), Algorithm 2 is presented. It should be pointed out that the optimal values of $\mathbf{w}$ in each step of Algorithm 2 can be achieved by using useful convex optimization packages such as CVX in MATLAB. Moreover, considering $M' = \sqrt{M}$, N_{opt} could be obtained as follows,

$$N_{opt} = \left\lfloor \frac{T_D}{t_r} - \frac{M'^2_{opt}}{f_s t_r} \right\rfloor \tag{39}$$

IV. NUMERICAL RESULTS AND DISCUSSION

In this section, we evaluate the proposed method and optimization problems through simulations. The values of the parameters used for the simulation are provided in Table 2.

The channel gains between the PU and the SARs are assumed to be slow and flat, following a standard complex Gaussian distribution with $\sigma_z^2 = 1$. We assume that the spectrum sensing operates in the low SNR regime, where $\sigma_s^2 = 0.2$.

To simulate the cost function and constraints of the problem (29), we select an arbitrary SAR to access the spectrum whenever the PU's state is determined to be idle by the FC. We separately simulate the average throughput of each user participating in the cooperative spectrum sensing in both the energy-surplus and energy-deficit modes.

In the energy-deficit mode, we study the behavior of the objective function and constraints of the optimization problem (29) with respect to the decision threshold (η) for different numbers of SARs. Figures 2 to 7 present the results.

Figure 2 illustrates the local throughput function of each SAR for seven different numbers of SARs ($N = 17, \ldots, 23$) that cooperate to sense the spectrum. The curves are obtained through both analytical analysis and Monte Carlo simulations. The simulations align well with the analysis curves. It is observed that there is a wide range of η values over which the curves exhibit concave behavior. As

Algorithm 2 Maximization of Throughput for Energy-Surplus Mode

Data: $f_0 = \infty$ and $N_{max} = \frac{T_D}{t_r} - 1$
Result: $f_{opt}, \mathbf{w}_{opt}, M'_{opt}$
for $N = 1{:}N_{max}$ **do**
  $M \leftarrow f_s(T_D - Nt_r)$ based on (2);
  $M' \leftarrow \sqrt{M}$;
  $\mathbf{w}_N \leftarrow$ the optimal value of $\mathbf{w}$;
  if $f_N(M',\mathbf{w}) < f_0$ **then**
    $f_{opt} \leftarrow f_N(M',\mathbf{w})$;
    $\mathbf{w}_{opt} \leftarrow \mathbf{w}_N$;
    $M'_{opt} \leftarrow M'$;
  end
  $f_0 \leftarrow f_{opt}(M',\mathbf{w})$
end

TABLE 2. Parameters for numerical simulations.

Parameter	value
f_s	10 kHZ
T_F	10 ms
t_r	0.2 ms
T_t	3 ms
p_s	2 mw
p_r	1.2 mw
p_t	10 mw
p_c	4 mw
p_u	38 mw
e_{saved}	0.5 mJ
$\bar{P}_c$	0.3
N	25
$\pi_1 = 1 - \pi_0$	0.6
ζ	0.8
E_0	0.6 mJ
C_t	2 Mbit/s

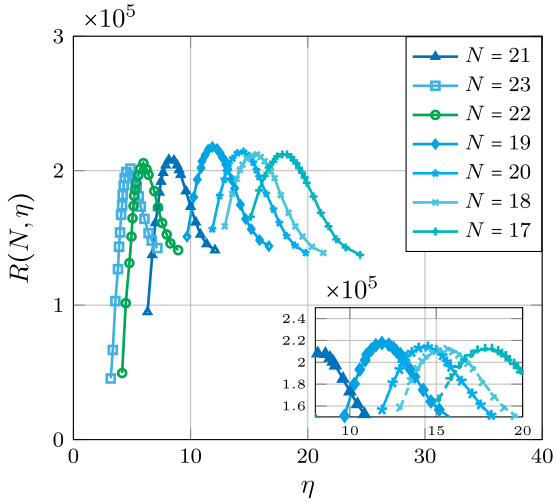

FIGURE 2. The throughput of each SAR for energy-deficit mode (29a) versus detection threshold when $\sigma_s^2 = 0.2$, $T_F = 10$ ms, $T_t = 5$ ms.

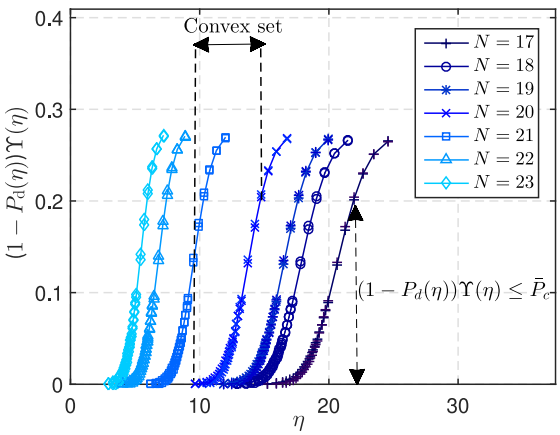

FIGURE 3. The probability of interference with the PU (29b) versus detection threshold for different number of SARs when $\sigma_s^2 = 0.2$, $T_F = 10$ *ms*, $T_t = 5$ *ms*.

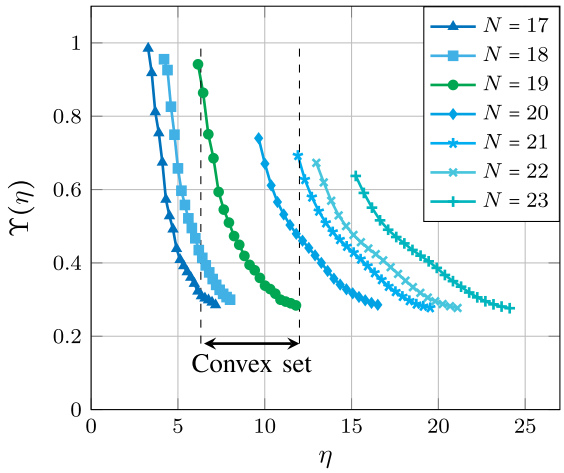

FIGURE 4. The normalized energy arrival rate versus detection threshold for different numbers of SARs when $\sigma_s^2 = 0.2$, $T_F = 10$ *ms*, $T_t = 5$ *ms*.

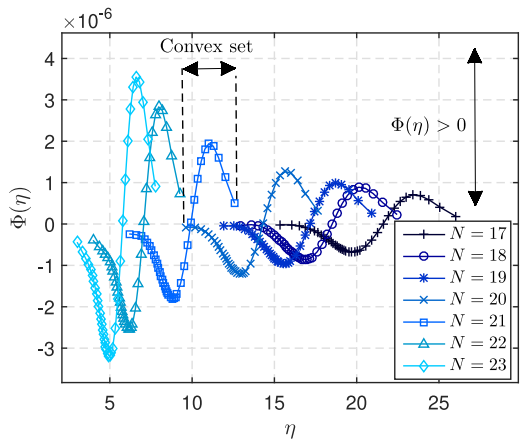

FIGURE 5. Constraint (29f) versus detection threshold for different number of SARs when $\sigma_s^2 = 0.2$, $T_F = 10$ *ms*, $T_t = 5$ *ms*.

the number of cooperating SARs increases, the number of samples gathered during the spectrum sensing interval decreases. This results in a decrease in the optimum decision threshold, as evident in the figure. Additionally, due to the trade-off between the number of SARs and the spectrum sensing interval, the throughput of the SARs reaches its maximum value at $N = 19$ and decreases for other values of N.

The probability of interference in the energy-deficit mode is illustrated in Figure 3. As seen, for the values of η which satisfy the constraints (29b), $(1 - P_{\rm d}(\eta))\Upsilon(\eta)$ is a convex function with respect to the decision threshold. In Figure 4, the normalized energy arrival rate for different numbers of SARs is depicted with respect to η. It is obvious that the constraint $(\Upsilon(\eta) \leq 1)$ is satisfied and the specified convex set determines the interval over which $\Upsilon(\eta)$ is a convex function with respect to η for different number of SARs. The constraint elicited from lemma 1, $\Phi(\eta) > 0$, versus η is demonstrated in Figure 5. Apparently, over the interval of η mentioned as convex set in the figure, $\Phi(\eta)$ meets the constraints $\Phi(\eta) > 0$ and $\frac{\partial^2 \Phi(\eta)}{\partial \eta^2} < 0$. The constraints extracted from lemma 2, $\Psi_1(\eta) < 0$ and $\Psi_2(\eta) < 0$, are illustrated in Figures 6 and 7, respectively. The same as previous constraints, these figures prove that over the intervals mentioned as a convex set the inequalities $\Psi_1(\eta) < 0$ and $\Psi_2(\eta) < 0$, and their convexity are satisfied for different numbers of SARs. To sum up, Figures 2–7 verify the accuracy of the analyses and convexity of the optimization problem (29).

In the case where the available energy in the battery is sufficient $(\Upsilon(\eta) > 1)$, the sensing operation follows a similar approach to OSA networks. Figure 8 illustrates the local throughput of each SAR as a function of variables M' and $\mathbf{w}^T\gamma$ for different values of σ_s^2. The figure confirms that the throughput is a concave function with respect to both M' and the weight coefficient vector $\mathbf{w}$. As expected, increasing the value of σ_s^2 leads to improved sensing performance and higher throughput accordingly.

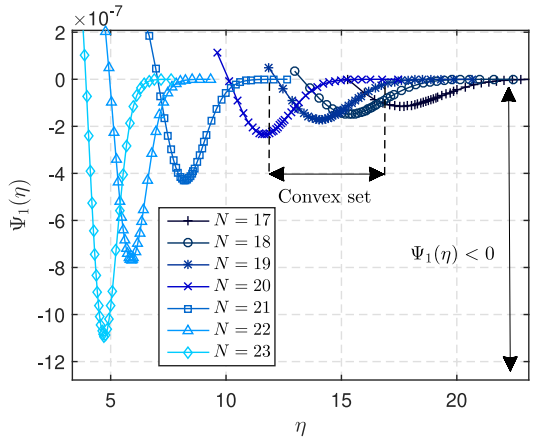

FIGURE 6. Constraint (29d) versus detection threshold for different number of SARs when $\sigma_s^2 = 0.2$, $T_F = 10$ *ms*, $T_t = 5$ *ms*.

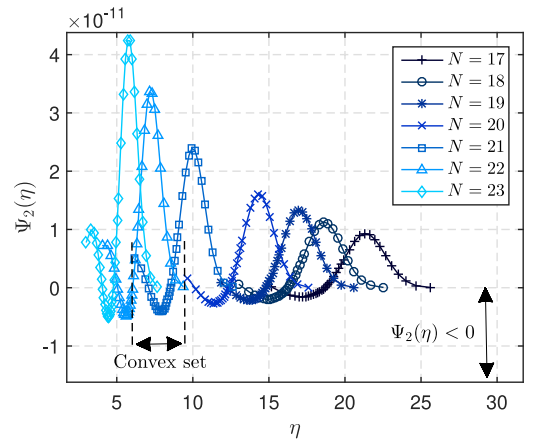

FIGURE 7. Constraint (29e) versus detection threshold for different number of SARs when $\sigma_s^2 = 0.2$, $T_F = 10$ *ms*, $T_t = 5$ *ms*.

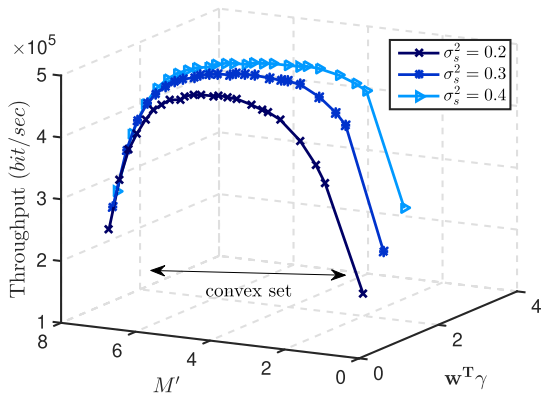

FIGURE 8. Local opportunistic throughput versus M' and $\mathbf{w}^T\gamma$ in different values of σ_s^2 when $T_F = 10$ *ms*.

We proceed to compare the ROC curves of the proposed system for both the energy-deficit and energy-surplus modes. Since the SARs are connected to a finite capacity battery, the sensing performance is affected by the normalized arrival energy factor, $\Upsilon(\eta)$. Figure 9 displays the ROC curve of the proposed energy harvesting system under the energy-deficit

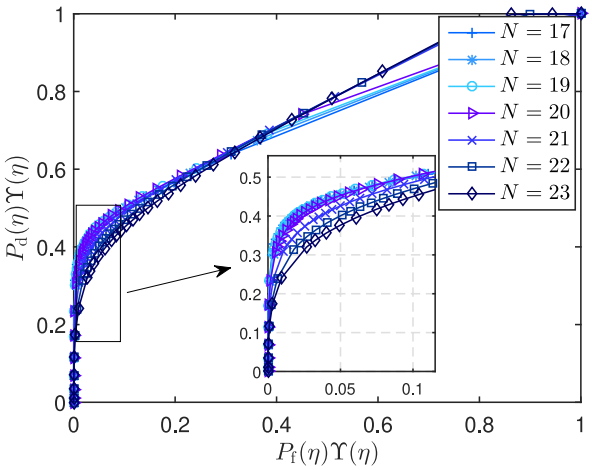

FIGURE 9. Probability of accessing idle spectrum versus probability of accessing the occupied spectrum for energy-deficit mode when $\sigma_s^2 = 0.2$, $T_F = 10$ *ms*, $T_t = 5$ *ms*.

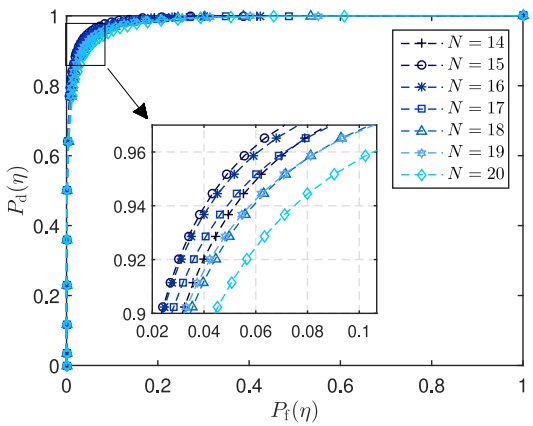

FIGURE 10. Different ROCs by varying number of SARs when $\sigma_p^2 = 0.2$ and $T_F = 10$ *ms* in surplus mode.

mode. It is evident from the figure that when the available energy in the battery is insufficient, the system's performance deteriorates significantly.

By comparing Figures 2 and 8, it can be observed that the deficiency of energy leads to a decrease in the throughput of each SAR to approximately half of the optimum throughput achievable in the energy-surplus mode.

Figure 10 presents the ROC of the system in the energy-surplus mode for different numbers of SARs. Due to the trade-off between the number of SARs and the sensing interval, the system's performance improves as the number of SARs increases from 14 to 15. However, from 15 to 20, the performance starts to degrade. Overall, the best sensing performance, regardless of the amount of consumed energy, is achieved when $N = 15$. However, considering the limitation of available energy, the optimum number of SARs for maximizing throughput is found to be $N = 19$.

Finally, we have compared different ROC curves of the proposed system model for two different weighting vectors in Figure 11. This figure provides $P_d(\eta)$ versus $P_f(\eta)$ for the obtained weighting vector $\mathbf{w}_{opt}$ in (23) and the equal gaining

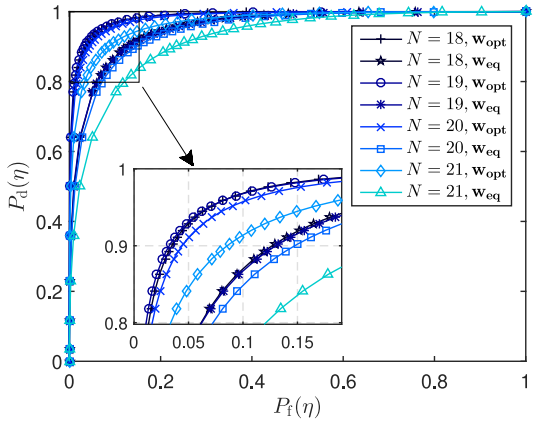

FIGURE 11. Comparison between ROCs for different numbers of users and weight coefficient vector, when $\sigma_p^2 = 0.2$ and $T_F = 10$ *ms*.

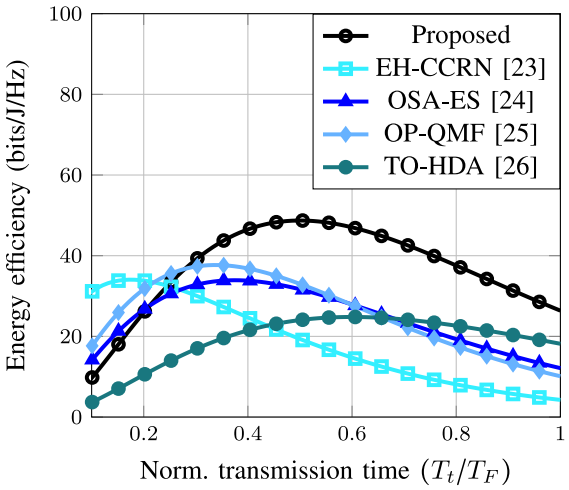

FIGURE 12. The comparison of EE in energy-surplus mode against normalized transmission time between the proposed algorithm and algorithms EH-CCRN in [23] and OSA-ES [24], OP-QMF [25], TO-HDA in [26] for $N = 20$, $T_F = 10$ *ms*.

vector $\mathbf{w}_{eq} \triangleq \frac{1}{N}\mathbf{1}$. It is clear that the area under the curve with $N_{opt} = 19$ and w_{opt} is larger than the others. Therefore, numerical results verify the improvement of the proposed model compared with the conventional models.

Figure 12 presents a comparison of EE in energy-deficit mode between our proposed algorithm and the algorithms EH-CCRN [23], OSA-ES [24], OP-QMF [25], and TO-HDA [26] with parameters set to $N = 20$ and $T_F = 10$ *ms*. Initially, for short transmission time slots where our proposed algorithm faces the decision of energy harvesting or transmission, it exhibits lower EE compared to the other two algorithms. However, as the transmission duration increases, the EE of our proposed algorithm shows improvement, eventually surpassing the performance of the other algorithms.

In addition, in Figure 13, we analyze the normalized achievable throughput as SE for different numbers of users in energy-surplus mode, comparing our proposed algorithm with the algorithms EH-CCRN, OSA-ES, OP-QMF, and TO-HDA while setting $T_t = 5$ *ms* and $T_F = 10$ *ms*. Notably,

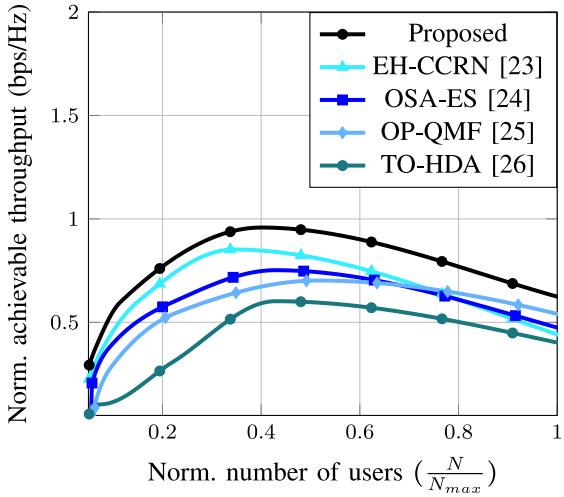

FIGURE 13. The comparison of achievable throughput as SE for different numbers of users in energy-surplus mode between the proposed algorithm and algorithms EH-CCRN [23], OSA-ES [24], OP-QMF [25], TO-HDA [26] for $T_t = 5$ *ms*, $T_F = 10$ *ms*.

our proposed algorithm enhances network throughput as the number of collaborating users increases, primarily due to improved detection accuracy. However, beyond a certain point, an interesting trend emerges: the throughput begins to decrease. This is attributed to the fact that increasing the number of collaborating users does not further enhance detection probability, yet it consumes additional energy. Consequently, this energy consumption leaves the SARs with less power for their own transmissions, resulting in reduced network throughput.

V. CONCLUSION

In this paper, we investigated an energy-harvesting wireless network where multiple SARs perform CSS to make decisions regarding the presence of PU within a limited time duration. Based on the CSS outcomes and the amount of energy stored in their batteries, the SARs can either remain active during this time frame or stay in sleep mode. Given the constraints of the limited time duration for CSS and the available energy resources, we formulated an optimization problem aimed at maximizing the throughput of each SAR while maintaining a specified interference probability level. We explored this optimization problem in both energy-deficit and energy-surplus scenarios.

For both modes, we applied convex optimization techniques to determine the optimal number of SARs, weighting vectors, and decision thresholds. This approach allowed us to achieve globally optimum values for these optimization parameters and the throughput function. Our numerical results in the energy-deficit mode revealed the existence of an interval where a pair of (N_{opt}, η_{opt}) and the corresponding optimal weight vector $\mathbf{w}_{opt}$ could be identified to maximize the throughput function. Similarly, in the energy-surplus mode, simulations demonstrated the presence of a specific point that maximized the throughput for each SAR. Therefore, our proposed scheme not only outperforms other

approaches in terms of EE but also enhances achievable throughput and SE significantly.

APPENDIX

A. DERIVATIVES OF THE PROBABILITIES

First, second, and fourth-order derivatives of probabilities of false alarm and detection can be derived and simplified as follows,

$$\frac{\partial P_{\mathrm{f}}}{\partial \eta} = \frac{-e^{-\frac{\alpha_f^2}{2}}}{\sqrt{2\pi M\sigma_z^4}} < 0, \quad \frac{\partial P_{\mathrm{d}}}{\partial \eta} = \frac{-\|\mathbf{C}^{-1}\boldsymbol{\gamma}\|e^{-\frac{\alpha_d^2}{2}}}{\sqrt{2\pi M\sigma_z^4\boldsymbol{\gamma}^T\mathbf{C}^{-1}\boldsymbol{\gamma}}} < 0 \tag{40}$$

$$\frac{\partial^2 P_{\mathrm{f}}}{\partial \eta^2} = \frac{\alpha_f e^{-\frac{\alpha_f^2}{2}}}{\sqrt{2\pi}M\sigma_z^4} > 0, \quad \frac{\partial^2 P_{\mathrm{d}}}{\partial \eta^2} = \frac{\|\mathbf{C}^{-1}\boldsymbol{\gamma}\|^2\alpha_d e^{-\frac{\alpha_d^2}{2}}}{\sqrt{2\pi}M\sigma_z^4\left(\boldsymbol{\gamma}^T\mathbf{C}^{-1}\boldsymbol{\gamma}\right)} < 0 \tag{41}$$

$$\frac{\partial^4 P_{\mathrm{f}}}{\partial \eta^4} = \frac{\left(\alpha_f^2-3\right)\alpha_f e^{-\frac{\alpha_f^2}{2}}}{\sqrt{2\pi}\left(M\sigma_z^4\right)^2} = \frac{\left(\alpha_f^2-3\right)}{M\sigma_z^4}\frac{\partial^2 P_{\mathrm{f}}}{\partial \eta^2} \tag{42}$$

$$\frac{\partial^4 P_{\mathrm{d}}}{\partial \eta^4} = \frac{\|\mathbf{C}^{-1}\boldsymbol{\gamma}\|^4\left(\alpha_d^2-3\right)\alpha_d e^{-\frac{\alpha_d^2}{2}}}{\sqrt{2\pi}\left(M\sigma_z^4\boldsymbol{\gamma}^T\mathbf{C}^{-1}\boldsymbol{\gamma}\right)^2} = \frac{\|\mathbf{C}^{-1}\boldsymbol{\gamma}\|^2\left(\alpha_d^2-3\right)}{M\sigma_z^4\boldsymbol{\gamma}^T\mathbf{C}^{-1}\boldsymbol{\gamma}}\frac{\partial^2 P_{\mathrm{d}}}{\partial \eta^2} \tag{43}$$

B. FUNCTION $(1-P_{\mathrm{D}}(\eta))\Upsilon(\eta)$ IS AN INCREASING FUNCTION

We observe that

$$(1-P_{\mathrm{d}}(\eta))\Upsilon(\eta) = \frac{e_{\mathrm{saved}}(1-P_{\mathrm{d}}(\eta))}{e_s+e_r+e_c+e_tP_{\mathrm{free}}} \tag{44}$$

Additionally,

$$\frac{\partial P_{\mathrm{free}}}{\partial \eta} = \frac{\partial}{\partial \eta}(\pi_0(1-P_{\mathrm{f}}(\eta))+\pi_1(1-P_{\mathrm{d}}(\eta))) = -\pi_0\frac{\partial P_{\mathrm{f}}(\eta)}{\partial \eta} - \pi_1\frac{\partial P_{\mathrm{d}}(\eta)}{\partial \eta} \tag{45}$$

Therefore, the first derivative of $(1-P_{\mathrm{d}}(\eta))\Upsilon(\eta)$ can be expressed as in (46), as shown at the bottom of this page. After simplification and referring to (42), it can be reformatted and expressed as (47), as shown at the bottom of this page. It is noteworthy that, based on (24) and (25) and considering practical scenarios, P_{f} and P_{d} are large and small, respectively. Thus, $(1-P_{\mathrm{d}}) < (1-P_{\mathrm{f}})$. This also implies that $\frac{e^{-\frac{\alpha_f^2}{2}}}{\sqrt{2\pi M\sigma_z^4}} < \frac{\|\mathbf{C}^{-1}\boldsymbol{\gamma}\|e^{-\frac{\alpha_d^2}{2}}}{\sqrt{2\pi M\sigma_z^4\boldsymbol{\gamma}^T\mathbf{C}^{-1}\boldsymbol{\gamma}}}$, and therefore the second term in the numerator is negligible compared to the first one, and the numerator is positive for practical cases. This concludes that this function is an increasing function of η.

C. CONVEXITY OF FUNCTION $(1-P_{\mathrm{D}}(\eta))\Upsilon(\eta)$

Streamlining constraint (19b) gives rise to the below inequality,

$$\Omega(\eta) \le 0. \tag{48}$$

Where,

$$\Omega(\eta) \triangleq (1-P_{\mathrm{d}}(\eta))\left(e_{saved}-\pi_1 e_t\bar{P}_c\right) - \bar{P}_c e_f - \bar{P}_c(e_t\pi_0)(1-P_{\mathrm{f}}(\eta)) \tag{49}$$

Second derivative of $\Omega(\eta)$ equals to $-\frac{\partial^2 P_{\mathrm{d}}}{\partial \eta^2}(e_{saved}-\pi_1 e_t\bar{P}_c)+\frac{\partial^2 P_{\mathrm{f}}}{\partial \eta^2}(\pi_0 e_t\bar{P}_c)$ which provided that $e_{saved} > \pi_1 e_t\bar{P}_c$, is obviously positive considering the sign of probabilities in Appendix A. So, the obtained condition results in the convexity of constraint (19b) with respect to η.

D. CONVEXITY OF $\Upsilon(\eta)$

Inequality $\Upsilon(\eta) < 1$ can be simplified as,

$$e_{saved} - e_f - \pi_0 e_t(1-P_{\mathrm{f}}(\eta)) - \pi_1 e_t(1-P_{\mathrm{d}}(\eta)) \le 0 \tag{50}$$

double differentiating from the left side of this inequality yields

$$\Phi(\eta) = \pi_0 e_t\frac{\partial^2 P_{\mathrm{f}}}{\partial \eta^2} + \pi_1 e_t\frac{\partial^2 P_{\mathrm{d}}}{\partial \eta^2} \tag{51}$$

It is obvious that (19c) would be a convex set, if and only if $\Phi(\eta) > 0$. Also, we should prove that the new constraint provides a convex set too. In this regard, the second derivative of (50) is

$$\frac{\partial^2 \Phi(\eta)}{\partial \eta^2} = \pi_0 e_t\frac{\partial^4 P_{\mathrm{f}}}{\partial \eta^4} + \pi_1 e_t\frac{\partial^4 P_{\mathrm{d}}}{\partial \eta^4} \tag{52}$$

which should be negative because of convexity of $-\Phi(\eta)$. Assuming $\alpha_f^2 < 1$, which is a practical assumption, $\alpha_f^2 - 3$ is negative. So, $\Phi(\eta) > 0$ can be rewritten as,

$$\frac{\partial}{\partial \eta}(1-P_{\mathrm{d}}(\eta))\Upsilon(\eta)) = e_{saved}\frac{\left(-\frac{\partial}{\eta}P_{\mathrm{d}}(\eta)\right)\{e_s+e_r+e_c+e_tP_{\mathrm{free}}\} - \left(\frac{\partial}{\eta}P_{\mathrm{free}}(\eta)\right))\{1-P_{\mathrm{d}}(\eta))\}}{(e_s+e_r+e_c+e_tP_{\mathrm{free}})^2} \tag{46}$$

$$= e_{saved}\frac{\frac{\|\mathbf{C}^{-1}\boldsymbol{\gamma}\|e^{-\frac{\alpha_d^2}{2}}}{\sqrt{2\pi M\sigma_z^4\boldsymbol{\gamma}^T\mathbf{C}^{-1}\boldsymbol{\gamma}}}(e_s+e_r+e_c+e_t\pi_0(1-P_{\mathrm{f}})) - e_t\pi_0(1-P_{\mathrm{d}})\frac{e^{-\frac{\alpha_f^2}{2}}}{\sqrt{2\pi M\sigma_z^4}}}{(e_s+e_r+e_c+e_tP_{\mathrm{free}})^2} > 0 \tag{47}$$

$$\pi_0 e_t \frac{\partial^2 P_{\rm f}}{\partial \eta^2} \frac{\left(\alpha_f^2-3\right)}{M\sigma_z^4} < -\pi_1 e_t \frac{\partial^2 P_{\rm d}}{\partial \eta^2} \frac{\left(\alpha_f^2-3\right)}{M\sigma_z^4} \tag{53}$$

Using (42) we have,

$$\pi_0 e_t \frac{\partial^4 P_{\rm f}}{\partial \eta^4} < -\pi_1 e_t \frac{\partial^2 P_{\rm d}}{\partial \eta^2} \frac{\left(\alpha_f^2-3\right)}{M\sigma_z^4} \tag{54}$$

Relaxing constraint $\frac{\partial^2\Phi(\eta)}{\partial\eta^2} < 0$ by replacing the upper bound of $\pi_0 e_t \frac{\partial^4 P_{\rm f}}{\partial \eta^4}$ from $\pi_0 e_t \frac{\partial^4 P_{\rm f}}{\partial \eta^4} < -\pi_1 e_t \frac{\partial^4 P_{\rm d}}{\partial \eta^4}$, the constraint $\frac{\partial^2\Phi(\eta)}{\partial\eta^2} < 0$ can be relaxed as,

$$\left(\alpha_f^2-3\right) < \frac{\|\mathbf{C}^{-1}\boldsymbol{\gamma}\|^2(\alpha_d^2-3)}{\boldsymbol{\gamma}^T\mathbf{C}^{-1}\boldsymbol{\gamma}} \Rightarrow \eta^2(a_\Phi)+\eta(b_\Phi)+c_\Phi < 0 \tag{55}$$

wherein, a_Φ and b_Φ and c_Φ are defined in (56), as shown at the bottom of this page.

Through straightforward yet tedious mathematical simplifications (omitted for the sake of brevity), it can be seen that $\Delta_\Phi \triangleq b_\Phi^2 - 4a_\Phi c_\Phi > 0$, and the quadratic function has two real solutions. Therefore, the interval that guarantees (55) is $\eta_L^{\Phi,1} < \eta < \eta_H^{\Phi,1}$, where

$$\eta_L^{\Phi,1} \triangleq \frac{-b_\Phi - \sqrt{b_\Phi^2 - 4a_\Phi c_\Phi}}{2a_\Phi}, \tag{58}$$

$$\eta_H^{\Phi,1} \triangleq \frac{-b_\Phi + \sqrt{b_\Phi^2 - 4a_\Phi c_\Phi}}{2a_\Phi}. \tag{59}$$

In addition, considering $\alpha_f^2 < 1$ gives rise to

$$\left(\|\mathbf{C}^{-1}\boldsymbol{\gamma}\|^2\right)\eta^2 - \left(2M\sigma_z^2\|\mathbf{C}^{-1}\boldsymbol{\gamma}\|\boldsymbol{\gamma}^T\mathbf{C}^{-1}\mathbf{1}\right)\eta + M\sigma_z^4\left[M\left(\boldsymbol{\gamma}^T\mathbf{C}^{-1}\mathbf{1}\right)^2 - 2\|\mathbf{C}^{-1}\boldsymbol{\gamma}\|^2\right] < 0 \tag{60}$$

which results $\eta_L^{\Phi,2} < \eta < \eta_H^{\Phi,2}$ where,

$$\eta_L^{\Phi,2} \triangleq M\sigma_z^2 \frac{\boldsymbol{\gamma}^T\mathbf{C}^{-1}\mathbf{1}}{\|\mathbf{C}^{-1}\boldsymbol{\gamma}\|} - \sqrt{2M}\sigma_z^2 \tag{61}$$

$$\eta_H^{\Phi,2} \triangleq M\sigma_z^2 \frac{\boldsymbol{\gamma}^T\mathbf{C}^{-1}\mathbf{1}}{\|\mathbf{C}^{-1}\boldsymbol{\gamma}\|} + \sqrt{2M}\sigma_z^2. \tag{62}$$

So,

$$max\left(\eta_L^{\Phi,1}, \eta_L^{\Phi,2}\right) < \eta < min\left(\eta_H^{\Phi,1}, \eta_H^{\Phi,2}\right) \tag{63}$$

provides a convex set of η for constraint (19c).

To sum up, under the assumption of $\Phi(\eta) > 0$ and (63), $\Upsilon(\eta) < 1$ is a convex set and the lemma is proved.

E. CONCAVITY OF OBJECTIVE FUNCTION (19a)

According to (41) and (40), $\frac{\partial^2 x(\eta)}{\partial\eta^2} < 0$, $\frac{\partial x(\eta)}{\partial\eta} > 0$, $\frac{\partial^2 y(\eta)}{\partial\eta^2} > 0$ and $\frac{\partial y(\eta)}{\partial\eta} > 0$, and so, the second derivative of (19a), which is shown in (57), as shown at the bottom of this page, is sum of positive and negative terms. Therefore, if we prove that one of the negative terms dominates the positive ones, the concavity of (19a) will be concluded. To this end, we aim to prove that,

$$\frac{\partial^2 x}{\partial\eta^2}\left(e_f+\pi_1 e_t y\right)\left[e_f+\pi_0 e_t x+\pi_1 e_t y\right] + 2\left(\pi_1 e_t x\frac{\partial y}{\partial\eta}\right)\left[\pi_0 e_t\frac{\partial x}{\partial\eta}+\pi_1 e_t\frac{\partial y}{\partial\eta}\right] < 0. \tag{64}$$

Should we rewrite the inequality as,

$$\frac{\partial^2 x}{\partial\eta^2}\left(e_f+\pi_1 e_t y\right)^2 + \pi_1 e_t x(\pi_0 e_t y\frac{\partial^2 x}{\partial\eta^2} + 2\pi_1 e_t(\frac{\partial y}{\partial\eta})^2) + \pi_0 e_t x\left(e_f\frac{\partial^2 x}{\partial\eta^2}+2\pi_1 e_t\frac{\partial y}{\partial\eta}\frac{\partial x}{\partial\eta}\right) < 0, \tag{65}$$

it can be readily observed if

$$\Psi_1(\eta) < 0, \;\; \Psi_2(\eta) < 0 \tag{66}$$

where,

$$\Psi_1(\eta) \triangleq e_f\frac{\partial^2 x}{\partial\eta^2} + 2\pi_1 e_t\frac{\partial y}{\partial\eta}\frac{\partial x}{\partial\eta} \tag{67}$$

$$\Psi_2(\eta) \triangleq \frac{\partial^2 x}{\partial\eta^2}\left(\left(e_f+\pi_1 e_t y\right)^2 + e_t^2\pi_1\pi_0 xy\right)$$

$$a_\Phi = \|\mathbf{C}^{-1}\boldsymbol{\gamma}\|^2\left(1-\frac{\|\mathbf{C}^{-1}\boldsymbol{\gamma}\|^4}{(\boldsymbol{\gamma}^T\mathbf{C}^{-1}\boldsymbol{\gamma})^2}\right), \quad b_\Phi = 2M\sigma_z^2\|\mathbf{C}^{-1}\boldsymbol{\gamma}\|\left(\frac{\|\mathbf{C}^{-1}\boldsymbol{\gamma}\|^4\boldsymbol{\gamma}^T\mathbf{C}^{-1}(\boldsymbol{\gamma}+\mathbf{1})}{\left(\boldsymbol{\gamma}^T\mathbf{C}^{-1}\boldsymbol{\gamma}\right)^2} - \boldsymbol{\gamma}^T\mathbf{C}^{-1}\mathbf{1}\right)$$

$$c_\Phi = M^2\sigma_v^4\left[\left(\boldsymbol{\gamma}^T\mathbf{C}^{-1}\mathbf{1}\right)^2 - \|\mathbf{C}^{-1}\boldsymbol{\gamma}\|^4\left(1-\frac{\boldsymbol{\gamma}^T\mathbf{C}^{-1}\mathbf{1}}{\boldsymbol{\gamma}^T\mathbf{C}^{-1}\boldsymbol{\gamma}}\right)^2\right] + 6M\sigma_v^4\|\mathbf{C}^{-1}\boldsymbol{\gamma}\|^2\left(\frac{\|\mathbf{C}^{-1}\boldsymbol{\gamma}\|^2}{\boldsymbol{\gamma}^T\mathbf{C}^{-1}\boldsymbol{\gamma}}-1\right). \tag{56}$$

$$\frac{\pi_0 C_t\frac{T_t}{T_F}}{\left(e_f+\pi_0 e_t x+\pi_1 e_t y\right)^3} \times \left(\left[\overbrace{\frac{\partial^2 x}{\partial\eta^2}\left(e_f+\pi_1 e_t y\right)}^{-}\overbrace{-\pi_1 e_t x\frac{\partial^2 y}{\partial\eta^2}}^{-}\right]\left[e_f+\pi_0 e_t x+\pi_1 e_t y\right] + 2\left[\overbrace{\pi_1 e_t x\frac{\partial y}{\partial\eta}}^{+}\overbrace{-\frac{\partial x}{\partial\eta}\left(e_f+\pi_1 e_t y\right)}^{-}\right]\left[\pi_0 e_t\frac{\partial x}{\partial\eta}+\pi_1 e_t\frac{\partial y}{\partial\eta}\right]\right) \tag{57}$$

$$+2\left(\pi_1 e_t \frac{\partial y}{\partial \eta}\right)^2 x, \tag{68}$$

Inequality (65) will be held. Now, we will initially prove that $\Psi_1(\eta) < 0$ provides a convex set, then considering this constraint, convexity of $\Psi_2(\eta) < 0$ can be concluded. Finally, the cost function (19a) would be concave under the assumption of constraints in (66).

Same as previous sections, assuming $\Psi_1(\eta) < 0$, we prove that $\Psi_1(\eta)$ is a convex function with respect to η. Defining $\Gamma(\eta) \triangleq \frac{\partial^2 \Psi_1(\eta)}{\partial \eta^2}$, we have,

$$\begin{aligned}\Gamma(\eta) = e_f \frac{\partial^4 x}{\partial \eta^4} + 4\pi_1 e_t \frac{\partial^2 y}{\partial \eta^2}\frac{\partial^2 x}{\partial \eta^2} + 2\pi_1 e_t \frac{\partial^3 y}{\partial \eta^3}\frac{\partial x}{\partial \eta} \\ + 2\pi_1 e_t \frac{\partial y}{\partial \eta}\frac{\partial^3 x}{\partial \eta^3}\end{aligned} \tag{69}$$

given the assumption ($\alpha_f^2 < 1$) mentioned before in Appendix C and using (42), we obtain

$$\begin{aligned} e_f \frac{\partial^2 x}{\partial \eta^2} &< -2\pi_1 e_t \frac{\partial y}{\partial \eta}\frac{\partial x}{\partial \eta} \implies \\ &\quad - 2\pi_1 e_t \frac{\partial x}{\partial \eta}\frac{\partial y}{\partial \eta}\frac{\left(\alpha_f^2 - 3\right)}{M\sigma_z^4} \\ &< \frac{\left(\alpha_f^2 - 3\right)}{M\sigma_z^4} e_f \frac{\partial^2 x}{\partial \eta^2} = e_f \frac{\partial^4 x}{\partial \eta^4} \end{aligned} \tag{70}$$

Also, the terms $\frac{\partial^3 x}{\partial \eta^3}$, $\frac{\partial^2 x}{\partial \eta^2}$, $\frac{\partial^3 y}{\partial \eta^3}$ and $\frac{\partial^2 y}{\partial \eta^2}$ in (69) can be streamlined as

$$\begin{aligned} \frac{\partial^2 x}{\partial \eta^2} &= \frac{-\alpha_f}{\sqrt{M\sigma_z^4}}\frac{\partial x}{\partial \eta}, \qquad \frac{\partial^3 x}{\partial \eta^3} = \frac{\left(\alpha_f^2 - 1\right)}{M\sigma_z^4}\frac{\partial x}{\partial \eta} \\ \frac{\partial^2 y}{\partial \eta^2} &= \frac{-\|\mathbf{C}^{-1}\boldsymbol{\gamma}\|\alpha_d}{\sqrt{M\sigma_z^4\left(\boldsymbol{\gamma}^T\mathbf{C}^{-1}\boldsymbol{\gamma}\right)}}\frac{\partial y}{\partial \eta}, \\ \frac{\partial^3 y}{\partial \eta^3} &= \frac{-\|\mathbf{C}^{-1}\boldsymbol{\gamma}\|^2\left(\alpha_d^2 - 1\right)}{M\sigma_z^4\left(\boldsymbol{\gamma}^T\mathbf{C}^{-1}\boldsymbol{\gamma}\right)}\frac{\partial y}{\partial \eta} \end{aligned} \tag{71}$$

Using in (70) and (71), inequalities (72) and subsequently (73), as shown at the bottom of this page, are obtained, where a_Ψ, b_Ψ and c_Ψ are defined in (74), as shown at the bottom of this page. As through intricate mathematical manipulations, it can be shown that $\Delta_\Psi \triangleq b_\Psi^2 - 4a_\Psi c_\Psi > 0$, obviously, (73) will hold if $\eta_L^\Psi < \eta < \eta_H^\Psi$, where

$$\begin{aligned}\eta_L^\Psi &\triangleq \frac{-b_\Psi - \sqrt{b_\Psi^2 - 4a_\Psi c_\Psi}}{2a_\Psi}, \eta_H^\Psi \\ &\triangleq \frac{-b_\Psi + \sqrt{b_\Psi^2 - 4a_\Psi c_\Psi}}{2a_\Psi}\end{aligned} \tag{75}$$

Now, after proving convexity of $\Psi_1(\eta) < 0$, we use it to prove convexity of $\Psi_2(\eta) < 0$. Using $\Psi_1(\eta) < 0$, the following inequality can be easily obtained,

$$2\left(\pi_1 e_t \frac{\partial y}{\partial \eta}\right)^2 x\frac{\partial x}{\partial \eta} < -e_f \pi_1 e_t x \frac{\partial^2 x}{\partial \eta^2}\frac{\partial y}{\partial \eta} \tag{76}$$

By multiplying variable $\frac{\partial x}{\partial \eta}$ in $\Psi_2(\eta) < 0$ and applying (76), the inequality $\Psi_2(\eta) < 0$ can be relaxed by its obtained upper bound as below,

$$\frac{\partial x}{\partial \eta}\frac{\partial^2 x}{\partial \eta^2}\left(\left(e_f + \pi_1 e_t y\right)^2 + e_t^2 \pi_1 \pi_0 xy\right) < e_f \pi_1 e_t \frac{\partial^2 x}{\partial \eta^2} x \frac{\partial y}{\partial \eta} \tag{77}$$

By streamlining the above inequality we have,

$$\frac{\partial x}{\partial \eta}\left[\left(e_f + \pi_1 e_t y\right)^2 + e_t^2 \pi_1 \pi_0 xy\right] - \pi_1 e_t e_f \frac{\partial y}{\partial \eta} x > 0. \tag{78}$$

Using $\alpha_f^2 < 1$, calculation indicates that this inequality has no limitation from the lower bound while the upper bound is restricted by $\eta < \eta_H^\Psi$ similar to $\Psi_1(\eta)$, and so, no additional condition is added to the problem. Therefore, to sum up, the obtained constraints for concavity of objective function (19a), under the assumption of $\Psi_1(\eta) < 0$, $\Psi_2(\eta) < 0$ and $max(\eta_L^{\Phi,2}, \eta_L^\Psi) < \eta < min(\eta_H^{\Phi,2}, \eta_H^\Psi)$, concavity of $R(\eta)$ on η is ensured.

$$\Gamma(\eta) > \frac{2\pi_1 e_t}{M\sigma_z^4}\left[\left(3 - \alpha_f^2\right) + \frac{2\alpha_f \alpha_d \|\mathbf{C}^{-1}\boldsymbol{\gamma}\|}{\sqrt{\boldsymbol{\gamma}^T\mathbf{C}^{-1}\boldsymbol{\gamma}}} + \frac{\left(\alpha_d^2 - 1\right)\|\mathbf{C}^{-1}\boldsymbol{\gamma}\|^2}{\boldsymbol{\gamma}^T\mathbf{C}^{-1}\boldsymbol{\gamma}} + \left(\alpha_f^2 - 1\right)\right]\frac{\partial x}{\partial \eta}\frac{\partial y}{\partial \eta} \tag{72}$$

$$2 + \frac{2\alpha_f \alpha_d \|\mathbf{C}^{-1}\boldsymbol{\gamma}\|}{\sqrt{\boldsymbol{\gamma}^T\mathbf{C}^{-1}\boldsymbol{\gamma}}} + \frac{\left(\alpha_d^2 - 1\right)\|\mathbf{C}^{-1}\boldsymbol{\gamma}\|^2}{\boldsymbol{\gamma}^T\mathbf{C}^{-1}\boldsymbol{\gamma}} > 0 \implies a_\Psi \eta^2 + b_\Psi \eta + c_\Psi > 0 \tag{73}$$

$$\begin{aligned} a_\Psi &\triangleq \|\mathbf{C}^{-1}\boldsymbol{\gamma}\|^2\left(2 + \frac{\|\mathbf{C}^{-1}\boldsymbol{\gamma}\|^2}{\boldsymbol{\gamma}^T\mathbf{C}^{-1}\boldsymbol{\gamma}}\right) \\ b_\Psi &\triangleq -2\|\mathbf{C}^{-1}\boldsymbol{\gamma}\|\left(M\boldsymbol{\gamma}^T\mathbf{C}^{-1}(\sigma_x^2\boldsymbol{h} + 2\sigma_z^2\mathbf{1})\right) - \frac{\|\mathbf{C}^{-1}\boldsymbol{\gamma}\|^2}{\boldsymbol{\gamma}^T\mathbf{C}^{-1}\boldsymbol{\gamma}} M\boldsymbol{\gamma}^T\mathbf{C}^{-1}\left(\sigma_x^2\boldsymbol{h} + \sigma_z^2\mathbf{1}\right) \\ c_\Psi &\triangleq M\sigma_z^4\left[2\left(\boldsymbol{\gamma}^T\mathbf{C}^{-1}\boldsymbol{\gamma}\right) - \|\mathbf{C}^{-1}\boldsymbol{\gamma}\|^2\right] + 2M^2\sigma_z^2\left(\boldsymbol{\gamma}^T\mathbf{C}^{-1}\mathbf{1}\right)\left[\boldsymbol{\gamma}^T\mathbf{C}^{-1}\left(\sigma_x^2\boldsymbol{h} + \sigma_z^2\mathbf{1}\right)\right] + \|\mathbf{C}^{-1}\boldsymbol{\gamma}\|^2 M^2 \frac{\left[\boldsymbol{\gamma}^T\mathbf{C}^{-1}\left(\sigma_x^2\boldsymbol{h} + \sigma_z^2\mathbf{1}\right)\right]^2}{\boldsymbol{\gamma}^T\mathbf{C}^{-1}\boldsymbol{\gamma}} \end{aligned} \tag{74}$$

$$\mathbf{H}=\frac{1}{\sqrt{2\pi}}\begin{pmatrix}\left(\mathbf{w}^T\boldsymbol{\gamma}\right)^2\xi\exp\left(-\xi^2/2\right) & -\boldsymbol{\gamma}^T\exp\left(-\xi^2/2\right)\left[1-M'\left(\mathbf{w}^T\boldsymbol{\gamma}\right)\xi\right]\\ -\boldsymbol{\gamma}\exp\left(-\xi^2/2\right)\left[1-M'\left(\mathbf{w}^T\boldsymbol{\gamma}\right)\xi\right] & M'^2\xi\exp\left(-\xi^2/2\right)\left(\boldsymbol{\gamma}\boldsymbol{\gamma}^T\right)\end{pmatrix}=\begin{pmatrix}a & \mathbf{b}^T\\ \mathbf{b} & \mathbf{D}\end{pmatrix} \tag{79}$$

F. CONVEXITY OF OPTIMIZATION PROBLEM (40)

According to [34], should the Hessian matrix defined as $\mathbf{H}\triangleq\nabla^2 f(M',\mathbf{w})$ be positive semi-definite, $g(M',\mathbf{w})=Q(\xi)$, where $\xi\triangleq Q^{-1}(1-\bar{P_C})\sqrt{1+2\boldsymbol{\gamma}_1}+M'\mathbf{w}^T\boldsymbol{\gamma}$, is a convex function on M' and $\mathbf{w}$. The Hessian matrix is calculated in the terms of M' and $\mathbf{w}$ in (79), as shown at the top of this page. Since a is positive, the Hessian matrix, $\mathbf{H}$, should be positive semi-definite matrix if and only if its Schur complement, $\mathbf{S}\triangleq\frac{a\mathbf{D}-\mathbf{b}\mathbf{b}^T}{a}$, is positive semi-definite [34]. Thus, the following constraint should be held,

$$\frac{M'^2\boldsymbol{\gamma}\boldsymbol{\gamma}^T\xi\exp\left(-\xi^2/2\right)}{\sqrt{2\pi}}-\frac{\boldsymbol{\gamma}\boldsymbol{\gamma}^T\exp\left(-\xi^2\right)\left(M'\xi\mathbf{w}^T\boldsymbol{\gamma}-1\right)^2}{\sqrt{2\pi}\left(\mathbf{w}^T\boldsymbol{\gamma}\right)^2\exp\left(-\xi^2/2\right)\xi}\succeq\mathbf{0}$$

which could be streamlined into $(2M'\xi\mathbf{w}^T\boldsymbol{\gamma}-1)\boldsymbol{\gamma}\boldsymbol{\gamma}^T\succeq\mathbf{0}$. Because the rank of the matrix $\boldsymbol{\gamma}\boldsymbol{\gamma}^T$ is 1, all of its eigenvalues is zero except the maximum one. So, $\boldsymbol{\gamma}\boldsymbol{\gamma}^T$ is a PSD matrix and we should merely ensure that $2M'\xi\mathbf{w}^T\boldsymbol{\gamma}-1\geq 0$ or

$$2M'\xi\mathbf{w}^T\boldsymbol{\gamma}-1\geq 0\Rightarrow\xi\geq\frac{1}{2M'\mathbf{w}^T\boldsymbol{\gamma}}0. \tag{80}$$

Using (37) and the fact that Q-function is a decreasing function on its parameter, we simplify (80) to $P_{\mathrm{f}}(M,\mathbf{w})\leq Q(\frac{1}{2M'\mathbf{w}^T\boldsymbol{\gamma}})$. So, we should find a lower bound for $Q(\frac{1}{2M'\mathbf{w}^T\boldsymbol{\gamma}})$ to ensure that $P_{\mathrm{f}}(M,\mathbf{w})$ is lower than this term. To this end, using (80) we can write,

$$2M'\mathbf{w}^T\boldsymbol{\gamma}\left(Q^{-1}(1-\bar{P_C})\sqrt{1+2\boldsymbol{\gamma}_1}+M'\mathbf{w}^T\boldsymbol{\gamma}\right)\geq 1$$

So, we obtain

$$\begin{aligned}&2Q^{-1}(1-\bar{P_C})\sqrt{1+2\boldsymbol{\gamma}_1}\left(M'\mathbf{w}^T\boldsymbol{\gamma}\right)\\&+2\left(M'\mathbf{w}^T\boldsymbol{\gamma}\right)^2-1\geq 0\end{aligned} \tag{81}$$

which is a quadratic function of $M'\mathbf{w}^T\boldsymbol{\gamma}$. It can be easily shown that the inequality can be solved as,

$$\begin{aligned}2M'\mathbf{w}^T\boldsymbol{\gamma}\geq&-Q^{-1}(1-\bar{P_C})\sqrt{1+2\boldsymbol{\gamma}_1}\\&+\sqrt{\left(Q^{-1}(1-\bar{P_C})\right)^2(1+2\boldsymbol{\gamma}_1)+2}\end{aligned} \tag{82}$$

Therefore, using (82) and $P_{\mathrm{f}}(M,\mathbf{w})\leq Q(\frac{1}{2M'\mathbf{w}^T\boldsymbol{\gamma}})$,

$$P_{\mathrm{f}}(M,\mathbf{w})\leq Q\left(\frac{1}{-Q^{-1}(1-\bar{P_C})\sqrt{1+2\boldsymbol{\gamma}_1}+\sqrt{\left(Q^{-1}(1-\bar{P_C})\right)^2(1+2\boldsymbol{\gamma}_1)+2}}\right) \tag{83}$$

can be concluded which makes the objective function of the optimization problem to be convex.

REFERENCES

[1] S. Greengard, *The Internet of Things*. Cambridge, MA, USA: MIT Press, 2021.

[2] A. Taherpour, M. Nasiri-Kenari, and S. Gazor, "Multiple antenna spectrum sensing in cognitive radios," *IEEE Trans. Wireless Commun.*, vol. 9, no. 2, pp. 814–823, Feb. 2010.

[3] L. Chettri and R. Bera, "A comprehensive survey on Internet of Things (IoT) toward 5G wireless systems," *IEEE Internet Things J.*, vol. 7, no. 1, pp. 16–32, Jan. 2020.

[4] H. Mokhtarzadeh, A. Taherpour, A. Taherpour, and S. Gazor, "Throughput maximization in energy limited full-duplex cognitive radio networks," *IEEE Trans. Commun.*, vol. 67, no. 8, pp. 5287–5296, Aug. 2019.

[5] M. Naderipour, A. Taherpour, A. Taherpour, and S. Gazor, "Design of optimal non-uniform quantizer in imperfect noisy reporting channels for collaborative spectrum sensing," *IEEE Trans. Veh. Technol.*, vol. 69, no. 11, pp. 12870–12882, Nov. 2020.

[6] E. Khorov et al., "Enabling the Internet of Things with Wi-Fi HaLow—Performance evaluation of the restricted access window," *IEEE Access*, vol. 7, pp. 127402–127415, 2019.

[7] A. Taherpour, M. Nasiri-Kenari, and S. Gazor, "Invariant wideband spectrum sensing under unknown variances," *IEEE Trans. Wireless Commun.*, vol. 8, no. 5, pp. 2182–2186, May 2009.

[8] A. Olutayo, Y. Dong, J. Cheng, J. F. Holzman, and V. C. M. Leung, "Performance of wireless powered communication systems over Beaulieu-Xie channels with nonlinear energy harvesters," *IEEE Open J. Commun. Soc.*, vol. 4, pp. 456–463, 2023.

[9] N. L. Johannsen, J. Mietzner, and P. A. Hoeher, "Joint communication and sensing using compressive sensing and a single multi-mode multi-port antenna," *IEEE Open J. Commun. Soc.*, vol. 5, pp. 71–82, 2024.

[10] E. Li, Y. Wang, Z. Liang, and M. Zheng, "Improving the security and reliability of energy-constrained two-way relay systems with nonlinear energy harvesting," *IEEE Access*, vol. 11, pp. 136793–136808, 2023.

[11] S. Dhanasekaran and T. Reshma, "Full-rate cooperative spectrum sharing scheme for cognitive radio communications," *IEEE Commun. Lett.*, vol. 22, no. 1, pp. 97–100, Jan. 2018.

[12] L. Hu, R. Shi, M. Mao, Z. Chen, H. Zhou, and W. Li, "Optimal energy-efficient transmission for hybrid spectrum sharing in cooperative cognitive radio networks," *China Commun.*, vol. 16, no. 6, pp. 150–161, Jun. 2019.

[13] R. Sawant and S. Nema, "SNR analysis in cooperative spectrum sensing for cognitive radio," in *Proc. Int. Conf. Adv. Commun. Comput. Technol. (ICACCT)*, 2018, pp. 392–396.

[14] H. Hu, H. Zhang, and Y.-C. Liang, "On the spectrum- and energy-efficiency tradeoff in cognitive radio networks," *IEEE Trans. Commun.*, vol. 64, no. 2, pp. 490–501, Feb. 2016.

[15] J. Ghosh et al., "A novel transceiver and an asynchronous mode for the hybrid multiple-access HetNet architecture," *IEEE Access*, vol. 11, pp. 135609–135625, 2023.

[16] E. C. Y. Peh, Y.-C. Liang, Y. L. Guan, and Y. Zeng, "Cooperative spectrum sensing in cognitive radio networks with weighted decision fusion schemes," *IEEE Trans. Wireless Commun.*, vol. 9, no. 12, pp. 3838–3847, Dec. 2010.

[17] Y. Zeng, Y. C. Liang, S. Zheng, and E. C. Y. Peh, "Optimal cooperative sensing and its robustness to decoding errors," in *Proc. IEEE Int. Conf. Commun. (ICC)*, Jun.2011, pp. 1–5.

[18] Y. Chen, "Optimum number of secondary users in collaborative spectrum sensing considering resources usage efficiency," *IEEE Commun. Lett.*, vol. 12, no. 12, pp. 877–879, Dec. 2008.

[19] S. Maleki, S. P. Chepuri, and G. Leus, "Energy and throughput efficient strategies for cooperative spectrum sensing in cognitive radios," in *Proc. IEEE 12th Int. Workshop Signal Process. Adv. Wireless Commun. (SPAWC)*, 2011, pp. 71–75.

[20] T. Sanislav, G. D. Mois, S. Zeadally, and S. C. Folea, "Energy harvesting techniques for Internet of Things (IoT)," *IEEE Access*, vol. 9, pp. 39530–39549, 2021.

[21] X. Huang, R. Yu, J. Kang, Z. Xia, and Y. Zhang, "Software defined networking for energy harvesting Internet of Things," *IEEE Internet Things J.*, vol. 5, no. 3, pp. 1389–1399, Jun. 2018.

[22] S. Guo and X. Zhao, "Deep reinforcement learning optimal transmission algorithm for cognitive Internet of Things with RF energy harvesting," *IEEE Trans. Cogn. Commun. Netw.*, vol. 8, no. 2, pp. 1216–1227, Jun. 2022.

[23] S. Chatterjee, S. P. Maity, and T. Acharya, "Energy-spectrum efficiency trade-off in energy harvesting cooperative cognitive radio networks," *IEEE Trans. Cogn. Commun. Netw.*, vol. 5, no. 2, pp. 295–303, Jun. 2019.

[24] Pratibha, K. H. Li, and K. C. Teh, "Optimal spectrum access and energy supply for cognitive radio systems with opportunistic RF energy harvesting," *IEEE Trans. Veh. Technol.*, vol. 66, no. 8, pp. 7114–7122, Aug. 2017.

[25] D. A. U. Villalonga, J. T. Gómez, and M. J. F.-G. García, "Optimal sensing policy for energy harvesting cognitive radio systems," *IEEE Trans. Wireless Commun.*, vol. 19, no. 6 pp. 3826–3838, Jun. 2020.

[26] X. Liu, B. Xu, X. Wang, K. Zheng, K. Chi, and X. Tian, "Impacts of sensing energy and data availability on throughput of energy harvesting cognitive radio networks," *IEEE Trans. Veh. Technol.*, vol. 72, no. 1, pp. 747–759, Jan. 2023.

[27] S. Park, H. Kim, and D. Hong, "Cognitive radio networks with energy harvesting," *IEEE Trans. Wireless Commun.*, vol. 12, no. 3, pp. 1386–1397, Mar. 2013.

[28] H. Zeb, A. Ghani, M. Gohar, A. Alzahrani, M. Bilal, and D. Kwak, "Location centric energy harvesting aware routing protocol for IoT in smart cities," *IEEE Access*, vol. 11, pp. 102352–102365, 2023.

[29] D. Van Leemput, A. Sabovic, K. Hammoud, J. Famaey, S. Pollin, and E. De Poorter, "Energy harvesting for wireless IoT use cases: A generic feasibility model and tradeoff study," *IEEE Internet Things J.*, vol. 10, no. 17, pp. 15025–15043, Sep. 2023.

[30] A. Taherpour, H. Mokhtarzadeh, and T. Khattab, "Optimized error probability for weighted collaborative spectrum sensing in time- and energy-limited cognitive radio networks," *IEEE Trans. Veh. Technol.*, vol. 66, no. 10, pp. 9035–9049, Oct. 2017.

[31] Y. C. Liang, Y. Zeng, E. C. Y. Peh, and A. T. Hoang, "Sensing-throughput tradeoff for cognitive radio networks," *IEEE Trans. Wireless Commun.*, vol. 7, no. 4, pp. 1326–1337, Apr. 2008.

[32] Z. Quan, S. Cui, A. H. Sayed, and H. V. Poor, "Optimal multiband joint detection for spectrum sensing in cognitive radio networks," *IEEE Trans. Signal Process.*, vol. 57, no. 3, pp. 1128–1140, Mar. 2009.

[33] A. H. Sayed, *Fundamentals of Adaptive Filtering*. New York, NY, USA: Wiley, 2003.

[34] S. Boyd and L. Vandenberghe, *Convex Optimization*. Cambridge, U.K.: Cambridge Univ. Press, 2004.